Static magnetic properties of metallic systems explored by μSR-Spectroscopy

Alex Schenck

Swiss Federal Institute of Technology (ETH)

1 Introduction

This chapter is intended to acquaint you with some of the possibilities provided by μSR-spectroscopy in the study of static magnetic properties in the paramagnetic or diamagnetic phase as well as in the magnetically ordered phase of metallic systems. Most of the material discussed concerns the paramagnetic phase where, as you will find out, quite a number of different properties can be studied. In general this involves transverse field (TF)-measurements and the determination of the μ^+-Knight shift. In this respect these studies have much in common with NMR-measurements. However μSR has the advantage that it is not plagued by the skin effect, that it can be applied to single crystals and that the μ^+, as a spin-$\frac{1}{2}$ probe, is only sensitive to magnetic interactions. A certain disadvantage arises from the fact that the μ^+ is not an innocent probe and that local magnetic properties may be modified by its presence. In contrast to NMR the μ^+ is generally found at an interstitial position and therefore probes the magnetic properties of the host crystal from a different perspective.

As regards the study of the magnetically ordered phase by zero-field (ZF)-μSR the usefulness of this technique rests in its complementary role to neutron scattering. While a direct unambiguous determination of some long range magnetic structure by μSR is in general impossible, given that μSR can only probe locally this structure, it is well suited to check on the structure determination by neutron diffraction, provided the μ^+-site is known. As we will see, this works well even in the case of rather complicated commensurate antiferromagnetic configurations as well as in incommensurate structures. However, structure determinations by neutron diffraction are also not always unambiguous and there are indeed a number of examples where the two techniques yield seemingly inconsistent results.

Most of the discussed examples concern rare earth- or U-based intermetallic compounds, among them a number of so called heavy fermion systems. However, it is not

our goal to discuss here the physics of heavy fermions or heavy electron compounds in any detail, rather the examples were chosen for their pedagogical value. Those of you, who are particularly interested in μSR-studies of heavy fermion systems are referred to Schenck (1993), Amato (1997), Yaouanc and Dalmas de Reotièr (1997) (see also Schenck and Gygax (1995) for a general review article on μSR-studies in magnetic materials).

2 Spectroscopy in para- and diamagnetic phases

2.1 Response of local moments and conduction electrons.

We begin with a brief summary on the magnetic response in a variety of different cases.

Applying an external magnetic field which may vary in time and space (*i.e.* $\mathbf{H} = \mathbf{H}(\mathbf{r}, t)$) to a single crystal, the crystal responds by becoming magnetised. The induced magnetisation $\mathbf{M}$ may be negative with respect to $\mathbf{H}$ (*i.e.* $\mathbf{M} \cdot \mathbf{H} < 0$) and we will speak of *diamagnetism* , or $\mathbf{M}$ may be positive ($\mathbf{M} \cdot \mathbf{H} > 0$) and we will speak of *paramagnetism.* The all important response function $\underline{\chi}$ is called susceptibility and is in general a tensor. In the linear response approximation we write for the time and spatially dependent magnetisation inside a sample of volume V (Jonas and March, 1973):

$$M_\beta(\mathbf{r}, t) = \sum_\alpha \int_V d\mathbf{r}' \int_{-\infty}^{t} \chi_{\alpha\beta}(\mathbf{r}, \mathbf{r}', t - t') H_\alpha(\mathbf{r}', t') dt'. \tag{2.1}$$

For a uniform and time independent external field we have

$$M_\beta(\mathbf{r}, t) = \sum_\alpha \chi_{\alpha\beta}(\mathbf{r}, t) H_\alpha \tag{2.2}$$

and the time independent induced magnetisation is

$$\overline{M}_\beta(\mathbf{r}) = \langle M_\beta(\mathbf{r}, t) \rangle = \sum_\alpha \chi_{\alpha\beta}(\mathbf{r}) H_\alpha. \tag{2.3}$$

This formula is important if we are interested in the distribution of the magnetisation inside a sample. Randomly implanted μ^+ will respond to this distribution. If we are merely interested in the average or bulk magnetisation we get

$$\overline{M}_\beta = \langle M_\beta(\mathbf{r}) \rangle = \sum_\alpha \chi^0_{\alpha\beta} H_\alpha, \tag{2.4}$$

The dynamical susceptibility introduced in Equation 2.1 is an important quantity which, via the response function $S(\omega, q)$, enters into the neutron magnetic scattering differential cross section [Jones and March (1973): Lovesey *et al.* (1990)]. It is also linked via the *fluctuation-dissipation theorem* with the spin lattice relaxation rate $1/T_1$ [Moriya (1963)].

The calculation of $\chi_{\alpha\beta}$ and its temperature dependence in thermodynamical equilibrium starts from the expression

$$\chi_{\alpha\beta} = \frac{\partial M_\alpha}{\partial H_\beta} = \frac{\partial^2 F}{\partial H_\alpha \partial H_\beta} \tag{2.5}$$

where F is the free energy (E = energy),

$$F = E - TS \tag{2.6}$$

and S is the entropy.

Below we discuss the magnetic susceptibility in several important cases.

2.1.1 Paramagnetism of N noninteracting local moments

In this section we consider N noninteracting local moments or spins $\mu_i(\mathbf{R}_i) = g_J\mu_B\mathbf{J}$ at the atomic positions $\mathbf{R}_i$. The energy of each moment in an external field along the z-axis is $E_i = mg_J\mu_B H_z$ with $-J \leq m \leq +J$. The population $N(m)$ of each level m is given by the Boltzmann factor *i.e.*

$$N(m) = N_0 \frac{\exp(-mg_J\mu_B H_z/kT)}{\sum_m \exp(-mg_J\mu_B H_z/kT)} \tag{2.7}$$

and hence

$$E = \sum_m N(m) mg_J\mu_B H_z. \tag{2.8}$$

The free energy F is given by Equation 2.6 or

$$F = -NkTln\left(\sum_m \exp(-mg_J\mu_B H_z/kT)\right) . \tag{2.9}$$

For $mg_J\mu_B H_z/kT \ll 1$ we arrive at

$$\chi_0 \cong \frac{N \cdot \sum_m m^2 g_J^2 \mu_B^2}{kT(2J+1)} = \frac{NJ(J+1)g_J^2\mu_B^2}{3kT} = \frac{C}{T} \tag{2.10}$$

where $C = \dfrac{NJ(J+1)g_J^2\mu_B^2}{3k}$ is the Curie constant.

If the Zeeman energies are not small compared with kT the induced magnetisation $M(H,T)$ is most generally given by

$$M(H,T) = Ng_J\mu_B B_J\left(\frac{g_J\mu_B JH}{kT}\right) \tag{2.11}$$

where B_J is the famous Brillouin function which can be expressed as

$$B_J(x) = \frac{2J+1}{2J}\cot\left(\frac{2J+1}{2J}x\right) - \frac{1}{2J}\cot\frac{x}{2J}. \tag{2.12}$$

There is now no linear dependence of M on H and we are outside of the linear response regime. For $x \ll 1$ Equation 2.10 is recovered.

2.1.2 Paramagnetism in the Weiss molecular field approximation.

Consider the Zeeman plus Heisenberg Hamiltonian for the i-th moment:

$$\mathcal{H}_i = g\mu_B\mathbf{S}(\mathbf{R}_i)\cdot\mathbf{H} + 2\sum_{j\neq i} J_{\mathbf{R}_i-\mathbf{R}_j}\mathbf{S}(\mathbf{R}_i)\cdot\mathbf{S}(\mathbf{R}_j), \tag{2.13}$$

where $J_{\mathbf{R}_i-\mathbf{R}_j}$ is a scalar spin-spin coupling constant (if dipole-dipole or spin-orbit coupling is to be considered $J_{\mathbf{R}_i-\mathbf{R}_j}$ would become a tensor). The sum extends over all other moments at positions $\mathbf{R}_j$. In the molecular field approximation we replace $\mathbf{S}(\mathbf{R}_j)$ by its

expectation or mean value $\langle S(\mathbf{R}_j)\rangle = \langle \mathbf{S}\rangle$ which will be the same at all positions $\mathbf{R}_j$. Hence we write

$$\sum_{j\neq i} J_{\mathbf{R}_i-\mathbf{R}_j}\mathbf{S}(\mathbf{R}_i)\cdot\mathbf{S}(\mathbf{R}_j) \cong \sum_{j\neq i} J_{\mathbf{R}_i-\mathbf{R}_j}\mathbf{S}(\mathbf{R}_i)\cdot\langle\mathbf{S}\rangle \tag{2.14}$$

and obtain

$$\mathcal{H}_i \cong g\mu_B\mathbf{S}(\mathbf{R}_i)\cdot\mathbf{H}_{\text{eff}}, \tag{2.15}$$

where

$$\mathbf{H}_{\text{eff}} = \mathbf{H} + \frac{2}{g\mu_B}\sum_{j\neq i} J_{\mathbf{R}_i-\mathbf{R}_j}\langle\mathbf{S}\rangle \tag{2.16}$$

is now an effective field acting on each moment. The expectation value $\langle\mathbf{S}\rangle$ follows from the induced magnetisation $M(\mathbf{R}_i)$:

$$\langle S\rangle = \frac{M(\mathbf{R}_i)}{g\mu_B} = \frac{M}{g\mu_B}. \tag{2.17}$$

On the other hand (see Equation 2.3) and taking χ_0 to be isotropic (Equation 2.10)

$$M(\mathbf{R}_i) = \chi_0 H_{\text{eff}} = \chi_0\left(H + \frac{2}{g^2\mu_B^2}\sum_{j\neq i} J_{\mathbf{R}_i-\mathbf{R}_j}M(\mathbf{R}_i)\right) \tag{2.18}$$

or

$$M(\mathbf{R}_i) = \frac{\chi_0 H}{1-\left(\frac{2\chi_0}{g^2\mu_B^2}\right)\sum_{j\neq i} J_{\mathbf{R}_i-\mathbf{R}_j}} \tag{2.19}$$

or

$$\chi_{\text{eff}} = \frac{\chi_0}{1-\left(\frac{2\chi_0}{g^2\mu_B^2}\right)\sum J_{\mathbf{R}_i-\mathbf{R}_j}} = \frac{C}{T-\Theta}, \tag{2.20}$$

where C is given by Equation 2.10 and Θ is the "paramagnetic" Curie temperature:

$$\Theta = \frac{2S(S+1)\sum_{j\neq i} J_{\mathbf{R}_i-\mathbf{R}_j}}{3k}. \tag{2.21}$$

Equations 2.19 or 2.20 are valid in the limit of high temperatures (linear response approximation, Equation 2.3 applies). For arbitrary temperatures we replace in Equation 2.11 H by H_{eff}. For $H = 0$ a spontaneous magnetisation will appear below the Curie temperature T_c which in the mean field approximation is identical to the "paramagnetic" Curie temperature Θ, defined in Equation 2.21.

2.1.3 Orbital Van Vleck paramagnetism

We now consider orbital Van Vleck paramagnetism in systems with 4f- or 5f-electron shells subject to crystalline electric field (CEF) splitting. The systems in question are rare earth or actinide metals or intermetallic compounds. The crystalline electric field interaction of the f-electrons is weaker than their spin-orbit coupling so that the total angular momentum J remains a good quantum number. To describe the magnetic response of the f-electrons one starts from the Hamiltonian

$$\mathcal{H} = \mathcal{H}_C + \mathcal{H}_Z \tag{2.22}$$

where $\mathcal{H}_C$ is the CEF-Hamiltonian and $\mathcal{H}_Z$ represents the Zeeman interactions in the presence of an applied field. The magnetic susceptibility is then given by

$$\chi_\alpha = N g_J^2 \mu_B^2 \frac{1}{Z} \left[\sum_{m \neq n} |\langle m|J_\alpha|n\rangle|^2 \frac{(1 - \mathrm{e}^{-\beta\Delta_{mn}}) e^{-\beta E_N}}{\Delta_{mn}} + \sum_n |\langle n|J_\alpha|n\rangle|^2 \beta e^{-\beta E_n} \right], \quad (2.23)$$

where $|n\rangle$ are eigenfunctions and E_n are eigenvalues of $\mathcal{H}_C$, $\Delta_{mn} = E_m - E_n$, $\beta = 1/kT$ and $Z = \sum_n e^{-\beta E_n}$ is the partition function. The second term in Equation 2.23 corresponds to Equation 2.10, but may be absent in the case of an even number of f-electrons in a nonmagnetic singlet state. At high temperatures it develops also a $1/T$ dependence (exchange coupling among different f-electron atoms is neglected here). The first term is the result of a field induced mixing of the CEF-Eigenstates. It may be the only contribution present at low temperatures in case of a singlet ground state system. In this case χ_α becomes temperature independent for $T \to 0$ (only the CEF-groundstate is populated).

2.1.4 Paramagnetism of conduction electrons

For not too strong fields and a free electron gas

$$\chi_S^0 = \mu_B^2 N(\varepsilon_F), \quad (2.24)$$

where $N(\varepsilon_F)$ is the density of states at the Fermi energy. This is called the Pauli spin susceptibility(see *e.g.* Jones and March (1973)).

Going beyond the linear approximation condition (*i.e.* admitting arbitrarily strong H, remember that the electrons move on Landau orbitals confined to the Fermi surface) the induced magnetisation will develop a term which is periodic in B^{-1} (known as the de Haas van Alphen (dHvA) effect). The magnetic susceptibility can then be written as [Abrikosov (1972)]

$$\chi_S = \chi_S^0 + \chi_{\mathrm{dHvA}} \quad (2.25)$$

with

$$\chi_{\mathrm{dHvA}} \propto \frac{T}{B^{5/2}} \frac{e^{-\kappa T_D/B}}{\sinh(\kappa T/B)} \sin\left(\frac{cS}{e\hbar B} \pm \frac{\pi}{4}\right) \quad (2.26)$$

in the case that only one extremal orbit on the Fermi surface perpendicular to $\mathbf{B}$ is involved. S is the area enclosed by this extremal orbit and T_D is the so called Dingle temperature, which takes into account that the Landau levels are broadened due to electron scattering. Actually Equation 2.26 includes both spin and orbital contributions. The effect is strongly temperature dependent and can only be observed at sufficiently low temperatures.

The dHvA-modulation of the induced magnetisation $\mathbf{M}$ gives rise to a curious phenomenon, namely the appearance of coexisting diamagnetic and paramagnetic domains provided that certain conditions are fulfilled (Condon, 1966). To understand this phenomenon consider the magnetic induction $\mathbf{B}$ in a thin long cylinder which, as usual, is given by

$$\mathbf{B} = \mathbf{H}_{\mathrm{ext}} + 4\pi\mathbf{M}(\mathbf{B}) \quad (2.27)$$

or

$$\mathbf{H}_{\mathrm{ext}} = \mathbf{B} - 4\pi\mathbf{M}(B). \quad (2.28)$$

$M(B)$ is periodic in $1/B, M(B) \propto \sin(2\pi F/B)$, but within a limited range of only a few dHvA-cycles near some properly chosen B_0 ($B_0 \ll F$, to be in the dHvA regime) we may write

$$\frac{1}{B} = \frac{1}{B_0 + \Delta B} = \frac{1}{B_0}\left(1 - \frac{\Delta B}{B_0}\right)$$

and hence

$$M(B) \propto \sin\left(\frac{2\pi F}{B_0^2}\Delta B\right) \tag{2.29}$$

is approximately periodic in B. Inserting Equation 2.29 into Equation 2.28we find that H_{ext} rises linearly with B on which an oscillating component is superimposed. There will be even maxima and minima if the condition

$$\frac{\partial H_{\text{ext}}}{\partial B} = 1 - 4\pi\frac{\partial M}{\partial B} = 0 \tag{2.30}$$

or

$$\chi_{\text{dHvA}} = \frac{\partial M}{\partial B} = \frac{1}{4\pi} \tag{2.31}$$

is fulfilled, *i.e.* that the dHvA-oscillations are of sufficient amplitude. In this case the dependence of H_{ext} on B is illustrated in Figure 2.1a From this figure we see immediately

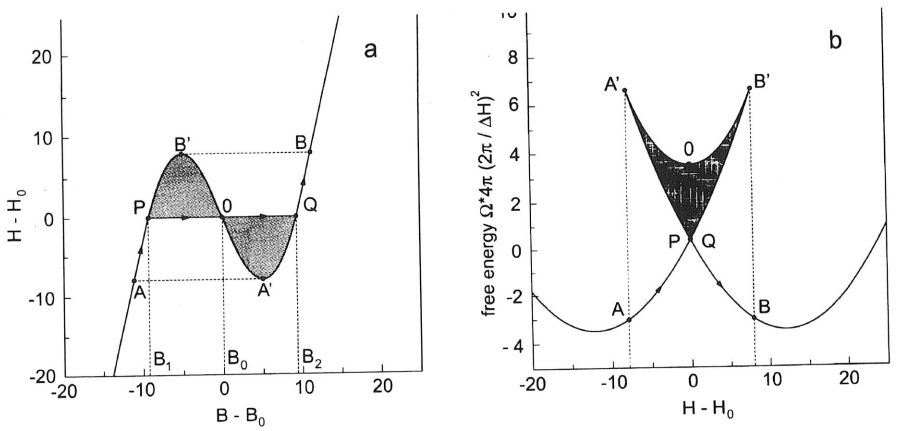

Figure 2.1. *(a) Correlation between H and the induction B in the range of one dHvA-cycle, (b) Dependence of free energy on external field H in the same range as in (a).*

that for certain values H_c, B may assume up to three values; B_1, B_0, B_2. The range between B_1 and B_2 is thermodynamically unstable since it belongs to a higher free energy (see Figure 2.1b). What happens is that upon increasing H_{ext} across H_c, B will jump from B_1 to B_2, *i.e.* from a diamagnetic to a paramagnetic behavior. Now let us consider a thin extended plate with $\mathbf{H}_{\text{ext}}$ perpendicular to the plate. In this case always

$$\mathbf{B} = \mathbf{H}_{\text{ext}}, \tag{2.32}$$

since the term $4\pi M$ is cancelled by the demagnetisation field $-N\mathbf{M}$ ($N = 4\pi$ for a thin plate). However, we have just learned that the range between B_1 and B_2 is forbidden. Hence the condition Equation 2.32 cannot be met in this range. How does the plate behave

in this case? It reacts in this case like a type I superconductor in the intermediate phase, namely the volume breaks up into alternating paramagnetic and diamagnetic domains with total volumes v_d, v_p such that

$$\overline{B} = \frac{v_d B_1 + v_p B_2}{v_d + v_p} = H_{\text{ext}} \tag{2.33}$$

and the free energy will always be at a minimum. Nothing is known about the spatial arrangement of the domains and their size. We will later see that μSR has provided the best available information on this phenomenon.

2.1.5 Magnetic response of conduction electrons in superconducting phases

As is well known in a BCS-superconductor electrons pair up into a singlet spin state, mediated by phonons, and a condensate of so called Cooper pairs is formed by opening up an energy gap on the Fermi surface. The energy gained in this way surpasses for not too large external fields ($H < H_{c2}$) the energy gain obtained by repopulating the spin up and spin down states with the result that for $T \to 0$K this repopulation is totally inhibited and the Pauli spin susceptibility will drop to zero. The actual temperature dependence of χ is described by the Yosida function (Yosida, 1958).

In contrast in a spin-triplet odd-parity superconductor the susceptibility is expected not to change with temperature below T_C.

2.1.6 Rudermann-Kittel-Kasuya-Yosida (RKKY) interaction

So far we have considered the direct effect of an external field on the spin polarisation or magnetisation of the conduction electrons. In the presence of local moments (*e.g.* provided by rare earth atoms) there will be an additional mechanism which will polarise the conduction electrons. This is the so called RKKY-mechanism.

Local moments with spin angular momentum $\mathbf{S}$ (*e.g.* f-electron moments) will interact with the conduction electrons with spin $\mathbf{s}$ by the exchange mechanism. This interaction is of the contact type and the Hamiltonian can be written as (Kittel, 1966)

$$\mathcal{H}_n = J(0) \sum_j \delta(\mathbf{r}_j - \mathbf{R}_n)\, \mathbf{s}_j \cdot \mathbf{S}_n, \tag{2.34}$$

where $J(0)$ is the exchange coupling constant and $\mathbf{R}_n$ the position of the local moment. The sum runs over over all conduction electrons. Representing the conduction electrons by plane waves the conduction electron spin density $\Delta\varrho(\mathbf{r})$ induced by the local moment at a distance $\mathbf{r}$ is calculated to be (Kittel, 1966)

$$\Delta\varrho(\mathbf{r}) = \varrho_\uparrow(\mathbf{r}) - \varrho_\downarrow(\mathbf{r}) = \frac{9\pi n}{2\varepsilon_F} J(0) S_z \sum_n F\left(2k_F(\mathbf{r} - \mathbf{R}_n)\right) \tag{2.35}$$

with

$$F(x) = \frac{x\cos x - \sin x}{x^4}, \tag{2.36}$$

where k_F is the Fermi momentum, n is the total density of conduction electrons (spin up and spin down). In order to induce a static spin polarisation $\Delta\varrho(\mathbf{r})$ the local moment has

to possess a nonzero expectation value of S_z. This can be induced by an external field. Assuming that the total angular momentum is given by $\mathbf{J}$ the external field $\mathbf{H}$ will induce a nonzero expectation value of J_z, which (see Equation 2.4) is

$$\langle J_z \rangle = \frac{\chi_f^{\text{at}} H}{g_J \mu_B}. \tag{2.37}$$

Here χ_f^{at} is, *e.g.* , the f-electron susceptibility per f-electron atom. $\langle S_z \rangle$ is obtained from the projection of $\mathbf{S}$ on $\mathbf{J}$ and $\mathbf{J}$ on $\mathbf{H}$.

$$\langle S_z \rangle = \frac{\mathbf{S} \cdot \mathbf{J}}{\sqrt{J(J+1)}} \frac{\langle J_z \rangle}{\sqrt{J(J+1)}} = (g_J - 1) J_z \tag{2.38}$$

and therefore

$$\langle S_z \rangle = \frac{g_J - 1}{g_J} \frac{\chi_f^{\text{at}} H}{\mu_B}. \tag{2.39}$$

This has to be inserted into Equation 2.35. The conduction electron polarisation as one moves away from a local moment assumes an oscillating behaviour, the famous RKKY oscillations. This position dependent polarisation takes place on top of the homogeneous polarisation arising from the Pauli paramagnetism. The total spin polarisation at a certain position is then given by

$$\Delta\varrho(r) = \frac{1}{\mu_B} \left(\chi_s + \underbrace{\frac{9\pi n}{2\varepsilon_F} J(0) \sum_n F(2k_F(\mathbf{r} - \mathbf{R}_n)}_{K(\mathbf{r})} \frac{(g_J - 1)}{g_J} \chi_f^{\text{at}} \right) H. \tag{2.40}$$

2.2 Hyperfine interactions and μ^+ Knight shift

2.2.1 Hyperfine fields at the μ^+

The interaction of the μ^+ (taking here the place of a nucleus) with an electron is most generally described by the Dirac equation. In the low energy limit we make use of the nonrelativistic Pauli approximation and obtain the Hamiltonian (Abragam, 1970)

$$\mathcal{H} \cong \frac{1}{2m} (\mathbf{p} - \frac{e}{c} \mathbf{A})^2 + g_e \mu_B \mathbf{S} \cdot \boldsymbol{\nabla} \times \mathbf{A} + e\varphi(r) \tag{2.41}$$

where $\mathbf{S}$ is the electron spin, $\mathbf{A} = \boldsymbol{\nabla} \times \left(\boldsymbol{\mu}_\mu / r \right)$ is the vector potential and $\boldsymbol{\mu}_\mu$ is the magnetic moment of the μ^+, given by $\boldsymbol{\mu}_\mu = g_\mu (e\hbar / 2m_\mu c) \mathbf{I}_\mu$.

After some manipulation we arrive at

$$\begin{array}{ccccccc} \mathcal{H} & = & \dfrac{\mathbf{p}^2}{2m} & + & e\varphi(r) & + & \mathcal{H}_1 \\ & & \uparrow & & \uparrow & & \uparrow \\ & & \text{kinetic} & & \text{potential} & & \text{magnetic} \\ & & \text{energy} & & \text{energy} & & \text{hyperfine} \\ & & & & & & \text{Hamiltonian} \end{array} + \begin{array}{c} \dfrac{e^2}{2mc} \mathbf{A}^2 \\ \uparrow \\ \text{negligibly} \\ \text{small} \end{array} \tag{2.42}$$

with

$$\begin{aligned}\mathcal{H}_1 &= \frac{e}{2mc}(\mathbf{p}\cdot\mathbf{A}+\mathbf{A}\cdot\mathbf{p}) + g_e\mu_B\mathbf{S}\cdot\boldsymbol{\nabla}\times\mathbf{A} \\ &= g_e\mu_B^e g_\mu\mu_B^\mu \mathbf{I}_\mu \left\{ \underbrace{\left(\frac{\mathbf{l}}{r^3}\right)}_{\text{orbital}} - \underbrace{\left(\frac{\mathbf{S}}{r^3} - \frac{3\mathbf{r}(\mathbf{S}\cdot\mathbf{r})}{r^5}\right)}_{\text{dipole-dipole}} + \underbrace{\frac{8\pi}{3}\mathbf{S}\delta(\mathbf{r})}_{\text{Fermi-contact}} \right\}. \end{aligned} \tag{2.43}$$

With respect to applications in solids we apply a *mean field approximation* and *replace* all electronic *operators* by their *expectation* values, *i.e.*

$$\mathbf{l} \longrightarrow \langle\mathbf{l}\rangle; \qquad \mathbf{S} \longrightarrow \langle\mathbf{S}\rangle \tag{2.44}$$

$\mathcal{H}_1$ looks then like a Zeeman interaction of the μ^+-spin $\mathbf{I}$ with the following effective fields:

Case 1

$$\mathbf{H}_{\text{orb}} = \frac{e}{mc}\frac{\langle\ell\rangle}{r^3}. \tag{2.45}$$

This is the field that is set up by an electron orbiting around the μ^+ at distance r with angular momentum $\langle\ell\rangle$. Such a situation has not been observed yet.

Case 2

$$\mathbf{H}^{\text{D}} = -g_e\mu_B\frac{1}{r^3}(\langle\mathbf{S}\rangle - \frac{3\mathbf{r}(\langle\mathbf{S}\rangle\cdot\mathbf{r})}{r^2}). \tag{2.46}$$

This is the dipole field generated by an electron at the μ^+ at a distance $\mathbf{r}$. The expectation value $\langle\mathbf{S}\rangle$, induced by an external field, can be written as (see Equations 2.4, 2.37)

$$\langle S_\beta\rangle = \frac{M_\beta^{\text{at}}}{2\mu_B} = \frac{1}{2}\frac{1}{\mu_B}\sum_{\alpha\beta}\chi_{\alpha\beta}^{\text{at}}H_\alpha, \tag{2.47}$$

where M_β^{at} and $\chi_{\alpha\beta}^{\text{at}}$ refer to the magnetisation or susceptibility per electron or per atom, to which the electron(s) may be attached. The effective dipole field can be expressed in the form

$$H_\beta^{\text{D}} = g_e\mu_B\sum_\alpha A_{\alpha\beta}^{\text{D}}\langle S\rangle_\alpha = \sum_{\alpha,\gamma}A_{\alpha\beta}^{\text{D}}(\mathbf{r})\chi_{\alpha\gamma}^{\text{at}}H_\gamma \tag{2.48}$$

or, in short

$$\mathbf{H}^{\text{D}} = \underline{\mathbf{A}}_i^{\text{D}}(\mathbf{r})\cdot(\underline{\boldsymbol{\chi}}^{\text{at}}\cdot\mathbf{H}), \tag{2.49}$$

where[1] $\underline{\mathbf{A}}^{\text{D}}$ and $\underline{\boldsymbol{\chi}}$ are now tensors. $\underline{\mathbf{A}}^{\text{D}}$ has generally the property that

$$\text{Tr}\,\underline{\mathbf{A}}^{\text{D}} = 0. \tag{2.50}$$

Inside a crystal the μ^+ will not only feel the dipole field from one neighbour electron, but from all electrons inside the volume V so that

$$\mathbf{H}^{\text{D}}(\mathbf{r}_\mu) = \frac{1}{V}\int_V \underline{\mathbf{A}}^{\text{D}}(\mathbf{r}_i-\mathbf{r}_\mu)(\underline{\boldsymbol{\chi}}^{\text{at}}(\mathbf{r}_i)\cdot\mathbf{H})\,dV \tag{2.51}$$

[1] the superscript D denotes a dipole term throughout the chapter

or

$$\mathbf{H}^{\mathrm{D}}(\mathbf{r}_\mu) = \sum_i \underline{\mathbf{A}}^{\mathrm{D}}(\mathbf{r}_i - \mathbf{r}_\mu)(\underline{\boldsymbol{\chi}}^{\mathrm{at}}(\mathbf{r}_i) \cdot \mathbf{H}) \tag{2.52}$$

in the case of local electron states at positions $\mathbf{r}_i$.

Case 3

$$\begin{aligned} \mathbf{H}_c &= \frac{8\pi}{3} g_e \mu_B \langle \mathbf{S} \rangle \delta(\mathbf{r}_\mu) \\ &= \frac{8\pi}{3} g_e \mu_B |\psi_e(\mathbf{r}_\mu)|^2 \langle \mathbf{S} \rangle; \end{aligned} \tag{2.53}$$

and, if $\langle \mathbf{S} \rangle$ is induced by an external field,

$$\begin{aligned} \mathbf{H}_c &= \frac{8\pi}{3} \langle |\psi_e(\mathbf{r}_\mu)|^2 \rangle_F \underline{\boldsymbol{\chi}}_s(\mathbf{r}_\mu) \cdot \mathbf{H}, \\ &= A_c \underline{\boldsymbol{\chi}}_s(\mathbf{r}_\mu) \cdot \mathbf{H}, \end{aligned} \tag{2.54}$$

where χ_s is defined with respect to one electron and $\langle |\psi_e(r_0)|^2 \rangle_F$ is the density of conduction electrons at the μ^+, averaged over the Fermi surface. This is the famous Fermi contact hyperfine field, which arises from the electronic spin density at the μ^+-position $\mathbf{r}_\mu$. In order to be effective, electronic wave functions have to overlap with the μ^+ like. With respect to the μ^+ there must be a s-wave component present in the electronic wave function.

2.2.2 Total field at the μ^+

The total field at implanted μ^+ in the presence of an external field $\mathbf{H}$ consists of microscopic (see preceding section) and macroscopic contributions. The macroscopic contributions are the demagnetisation field $\mathbf{B}_{\mathrm{dm}}$ and the Lorentz field $\mathbf{B}_L$. The demagnetisation field depends on the bulk magnetisation $\mathbf{M}_b$ and the shape of the sample

$$\mathbf{B}_{\mathrm{dm}} = -\underline{\mathbf{N}} \cdot \mathbf{M}_b, \tag{2.55}$$

where $\underline{\mathbf{N}}$ is again a tensor and is called demagnetisation factor. $\underline{\mathbf{N}}$ can be calculated analytically for an ellipsoid. For cylindrically or brick-shaped samples tabulated approximate values are available (Akishin, Gaganov, 1992). For a sphere one gets $N = 4\pi/3$, for an infinitely long cylinder with $\mathbf{H}$ parallel to the axis: $N_\parallel = 0$, or with $\mathbf{H}$ perpendicular to the axis: $N_\perp = 2\pi$, for an infinitely extended thin plate with $\mathbf{H}$ perpendicular to the plane: $N_\perp = 4\pi$.

The Lorenz field

$$\mathbf{B}_L = \frac{4\pi}{3} \mathbf{M}_b \tag{2.56}$$

arises when combining continuum theory with microscopic features. To this end one cuts out a fictitious sphere (the Lorentz sphere) around the μ^+ (this leads to $\mathbf{B}_L$) and refills it with all the microscopic sources of fields associated with local moments and spin densities discussed in the previous section. In total then

$$\mathbf{B}_\mu(\mathbf{r}_\mu) = \mathbf{H} + \left(\frac{4\pi}{3} \underline{\mathbf{E}} - \underline{\mathbf{N}} \right) \cdot \mathbf{M}_b + \mathbf{B}_{\mathrm{hf}}(\mathbf{r}_\mu), \tag{2.57}$$

where $\underline{\mathbf{E}}$ is the unit tensor and $\mathbf{B}_{\mathrm{hf}}(\mathbf{r}_\mu)$ may be composed of dipolar contributions (Equations 2.51 and 2.52 with the integral or the sum extending over the Lorentz sphere) and the contact hyperfine field (Equation 2.54).

2.2.3 The muon Knight Shift

The μ^+ Larmor frequency is given by $\omega_\mu = \gamma_\mu \cdot \mathbf{B}_\mu(\mathbf{r}_\mu)$ where $\gamma_\mu = 13.553879\text{kHz/G}$ ($\pm 0.5\text{ppm}$). Neglecting $\mathbf{B}_{\text{dm}}$ and $\mathbf{B}_L$ for the sake of argument, we get from Equation 2.57

$$\begin{aligned} \omega_\mu &= \gamma_\mu \sqrt{[\mathbf{H} + \mathbf{H}^{\text{D}}(\mathbf{r}_\mu) + \mathbf{H}_c(\mathbf{r}_\mu)]^2} \\ &= \gamma_\mu H \sqrt{1 + \frac{2}{H^2}(\mathbf{H}^{\text{D}} + \mathbf{H}_c) \cdot \mathbf{H} + \frac{1}{H^2}(\mathbf{H}^{\text{D}} + \mathbf{H}_c)^2} \end{aligned} \tag{2.58}$$

Because $|\mathbf{H}| \gg |\mathbf{H}^{\text{D}}|, |\mathbf{H}_c|$ (χ is small)

$$\begin{aligned} \omega_\mu &\cong \gamma_\mu H \sqrt{1 + \frac{2}{H^2}(\mathbf{H}^{\text{D}} + \mathbf{H}_c) \cdot \mathbf{H}} \\ &\cong \gamma_\mu \left(H + \frac{1}{H}(\mathbf{H}^{\text{D}} + \mathbf{H}_c) \cdot \mathbf{H} \right), \end{aligned} \tag{2.59}$$

i.e. only the projection of $\mathbf{H}^{\text{D}}$ and $\mathbf{H}_c$ on $\mathbf{H}$ will in first order contribute to ω_μ. This extra field $(\mathbf{H}^{\text{D}} + \mathbf{H}_c) \cdot \mathbf{H}/H$ is called the Knight shift and $K = (\mathbf{H}^{\text{D}} + \mathbf{H}_c) \cdot \mathbf{H}/H^2$ is called the Knight shift constant. With Equations 2.47, 2.51, 2.52 and 2.54 we now write

$$K = \frac{1}{H^2} \left\{ \mathbf{H} \cdot \left[\underline{\mathbf{A}}^{\text{D}}(\mathbf{r}_\mu) \cdot (\underline{\boldsymbol{\chi}}^{\text{at}} \cdot \mathbf{H}) + \frac{1}{\mu_B} A_c \underline{\boldsymbol{\chi}}_s \cdot \mathbf{H} \right] \right\}, \tag{2.60}$$

where

$$\underline{\mathbf{A}}^{\text{D}}(\mathbf{r}_\mu) = \sum_i \underline{\mathbf{A}}^{\text{D}}(\mathbf{r}_i - \mathbf{r}_\mu) \tag{2.61}$$

and $\sum_i$ is a lattice sum (or integral). $\underline{\mathbf{A}}^{\text{D}}(\mathbf{r}_\mu)$ depends on the assumed μ^+ lattice site and is further determined by symmetry properties of this site. For an axially symmetric site one gets

$$K^{\text{D}}_{\text{ax}} = \frac{1}{3} A^{\text{D}} \left[(\chi_\parallel - \chi_\perp) + (\chi_\perp + 2\chi_\parallel) P_2^0(\cos\theta) \right]. \tag{2.62}$$

The angle θ is the angle between $\mathbf{H}$ and the axis of axial symmetry. Generally, the angular dependence of K^{D} in Equation 2.60 involves only direction cosines in second order. In compounds containing localised *d*- or *f*-electrons χ will essentially arise only from those electrons. In compounds with an isotropic susceptibility (*e.g.* in cubic systems) the dipolar fields will not lead to an *isotropic* contribution to the Knight shift, *i.e.* in polycrystalline samples the Knight shift, or the average field, will not be influenced by dipolar interactions. However, there will be a distribution in dipolar fields which will cause relaxation (in NMR this is called powder broadening (Carter, Bennet, Kohan, 1977)).

As was mentioned before, the contact hyperfine interaction requires a nonzero spin density at the μ^+-site which is usually only fulfilled in metals. The corresponding Knight shift K_{s} will be written as (see Equations 2.54, 2.59):

$$K_{\text{s}} = \frac{8\pi}{3} \langle |\psi(\mathbf{r}_\mu)|^2 \rangle_F \chi_{\text{s}}/n, \tag{2.63}$$

where we have assumed an isotropic spin susceptibility χ_{s} (measured in emu/cm^3) and n is the conduction electron density). The charge density $\langle |\psi(\mathbf{r}_\mu)|^2 \rangle_F$ in the presence of the

muon is enhanced considerably over the value of n in the absence of the μ^+. This is due to the strong Coulomb interaction of the μ^+ and the conduction electrons which leads to a screening of the μ^+ charge and an actual charge distribution around the μ^+ similar to the charge distribution in atomic hydrogen. Note, however, that no paramagnetic state like muonium is formed since the screening of the μ^+ charge involves many conduction electrons and not just one. In addition the magnetic response of the electrons in the screening cloud may be different from the bulk behavior. A better way to write the Knight shift is the following:

$$\begin{aligned} K &= \frac{8\pi}{3}\mu_B \frac{n^{\uparrow}(\mathbf{r}_\mu) - n^{\downarrow}(\mathbf{r}_\mu)}{n_0^{\uparrow} - n_0^{\downarrow}}(n_0^{\uparrow} - n_0^{\downarrow})\frac{1}{H} = \frac{8\pi}{3}\alpha(\mathbf{r}_\mu)\chi_{\mathrm{s}} \\ &= \frac{A_{\mathrm{s}}}{\mu_B}\frac{\chi_{\mathrm{s}}}{n} \qquad (\chi_{\mathrm{s}} \text{ in emu/cm}^3) \,, \end{aligned} \tag{2.64}$$

where $n^{\uparrow}(\mathbf{r}_\mu) - n^{\downarrow}(\mathbf{r}_\mu)$ is the actual spin density at the μ^+ and $n_0^{\uparrow} - n_0^{\downarrow}$ is the undisturbed spin density. The spin density enhancement factor $\alpha(\mathbf{r}_\mu)$ has to be provided by theory. So far so-called spherical solid model (SSM) jellium calculations have given probably the most reliable results for μ^+ or protons in simple metals (Maninen+Nieminen, 1979; Maninen, 1983). The coupling constant A_{s} is an effective hyperfine field per unpaired electron. In any case measurements of the contact Knight shift K_{s} address in the first place properties induced by the presence of the μ^+. In this respect such studies contribute to an understanding of the local electronic structure of hydrogen in metals (Gygax *et al.*, 1984, Schenck 1981).

In f-electron compounds the RKKY interaction will induce an additional spin polarisation of the conduction electrons, as we have discussed in Section 2.1.6. In the μ^+ Knight shift this will be reflected by taking into account Equation 2.40:

$$\begin{aligned} K_f &= \frac{8\pi}{3}\mu_B\alpha(\mathbf{r}_\mu)\Delta\rho(\mathbf{r}_\mu) = \frac{8\pi}{3}\alpha(\mathbf{r}_\mu)\left\{\chi_{\mathrm{s}} + K(\mathbf{r}_\mu)\frac{g_J - 1}{g_J}\chi_f^{\mathrm{at}}\right\} H \\ &= K_{\mathrm{s}}\left\{1 + \frac{9\pi n}{2\varepsilon_F}\frac{1}{\chi_{\mathrm{s}}}J(0)\sum_n F(2\mathbf{k}_F\cdot(\mathbf{r}_\mu - \mathbf{R}_n))\frac{g_J - 1}{g_J}\chi_f^{\mathrm{at}}\right\}. \end{aligned} \tag{2.65}$$

For a free electron gas

$$\chi_{\mathrm{s}} = \mu_B^2 N(\varepsilon_F) = \mu_B^2\frac{3n}{2\varepsilon_F}\ [\mathrm{emu/cm}^3],$$

and hence

$$K_f = K_{\mathrm{s}}\left\{1 + 3\pi J(0)\sum_n F(2\mathbf{k}_F\cdot(\mathbf{r}_\mu - \mathbf{R}_n)\frac{g_J - 1}{g_J}\frac{\chi_f^{\mathrm{at}}}{\mu_B^2}\right\}. \tag{2.66}$$

From this equation we recognise that it should become possible to learn something about the very important exchange coupling constant $J(0)$ from measurements of K_f. What needs to be known is the Knight shift constant K_{s}. Information on K_{s} may be obtained from measurements of isostructural compounds in which the rare earth or actinide atom is replaced by nonmagnetic La or Th. Also the high temperature limit of K_f may yield directly K_{s} because of $\chi_f \propto (1/T) \to 0$.

So far we have assumed that $\chi_s(\mathbf{r})$ or $\chi_f^{at}(\mathbf{r})$ are independent of $\mathbf{r}$ and given by the bulk susceptibility (*i.e.* $\chi_f^{at} = \chi_f^{mol}/N_a$). However, this may not be true and we have to start from Equation 2.3 when calculating locally induced moments.

Finally we mention a rather small but nevertheless not always negligible effect which arises from the diamagnetism of the screening cloud around the μ^+. This is also known as the chemical shift and should be observable quite generally in solids and liquids in which the μ^+ is bound chemically into a diamagnetic state (all electron spins are paired up.). The shift constant sccan be calculated from the Lamb expression (Davies, 1967) and involves the calculation of the expectation value of $1/r$ of the electron distribution around the μ^+:

$$\sigma_{cs} = -\frac{e^2}{3mc^2}\langle r^{-1}\rangle. \tag{2.67}$$

σ_{cs} has been calculated for μ^+ in simple metals on the basis of a jellium approach (Zaremba and Zobin, 1980). The results as a function of conduction electron density are shown in Figure 2.2. The shifts are close to the value for atomic hydrogen (≈ -18ppm), underlining the very similar electron distribution in both cases.

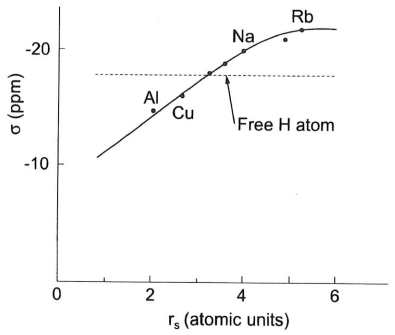

Figure 2.2. *Chemical shift constant σ for μ^+ in metals as a function of the electron density parameter $r_s = (3/4\pi n_0)^{1/2}/a_B$, (from Zaremba and Zobin, 1980).*

2.3 Determination of μ^+-site

As pointed out in the previous section the dipolar contribution to the Knight shift

$$K^D = \frac{1}{H^2}\mathbf{H}\cdot\underline{\mathbf{A}}^D\cdot\underline{\chi}\cdot\mathbf{H} \tag{2.68}$$

depends on the crystal structure of the considered system and the involved μ^+-site via the dipolar coupling tensor (see Equation 2.61)

$$\underline{\mathbf{A}}^D = \sum_i A^D(\mathbf{r}_i - \mathbf{r}_\mu), \tag{2.69}$$

where the sum extends over all μ^+ neighbor positrons $\mathbf{r}_i$. The sum will vanish for a μ^+-site with cubic point symmetry. In all other cases $\underline{\mathbf{A}}^D \neq 0$. Usually $\underline{\mathbf{A}}^D$ is calculated in a coordinate system fixed to the crystal. In general $\underline{\mathbf{A}}^D$ will contain also off diagonal

elements. By diagonalising $\underline{\mathbf{A}}^{\mathrm{D}}$ the local symmetry axes of a particular μ^+-site can be determined. In particular it may turn out that crystallographically equivalent sites are magnetically inequivalent, *i.e.* different $\underline{\mathbf{A}}_p^{\mathrm{D}}$ are involved, leading to the appearance of a split TF-μSR signal. The sum over these sites will reflect the overall symmetry of the crystal, *e.g.* in a cubic system

$$\sum_p \underline{\mathbf{A}}_p^{\mathrm{D}} = 0$$

For later use we present below the explicit dependence of K^{D} on the orientation of $\mathbf{H}$ with respect to the crystal axes $\underline{e}_x$, $\underline{e}_y$, $\underline{e}_z$, *i.e.* $\mathbf{H} = H(\sin\theta\sin\varphi\,\underline{e}_x + \sin\theta\cos\varphi\,\underline{e}_y + \cos\theta\,\underline{e}_z)$, following from Equation 2.68:

$$\begin{aligned} K^{\mathrm{D}}(\theta,\varphi) \;=\; & \frac{1}{3}(A^{xx}\chi_x + A^{yy}\chi_y + A^{zz}\chi_z) \\ & + \frac{2}{3}(A^{zz}\chi_z - \frac{1}{2}(A^{xx}\chi_x + A^{yy}\chi_y))P_2^0(\cos\theta) \\ & + \frac{1}{3}A^{xz}(\chi_x + \chi_z)P_2^1(\cos\theta)\cos\varphi \\ & + \frac{1}{3}A^{yz}(\chi_y + \chi_z)P_2^1(\cos\theta)\sin\varphi \\ & + \frac{1}{6}(A^{xx}\chi_x - A^{yy}\chi_y)P_2^2(\cos\theta)\cos 2\varphi \\ & + \frac{1}{6}A^{xy}(\chi_x + \chi_y)P_2^2(\cos\theta)\sin 2\varphi \end{aligned} \tag{2.70}$$

where the $P_2^i(\cos\theta)$ are the associated Legendre polynomials. It is hereby assumed that $\underline{\boldsymbol{\chi}}$ is diagonal in the chosen coordinate system.

We will now discuss two examples which show how the measurement of $\underline{\mathbf{A}}^{\mathrm{D}}$ will allow to determine the μ^+-site. It is obvious that this requires single crystal samples.

The first example concerns UPd_2Al_3, an interesting heavy fermion system which shows antiferromagnetic (AF) order below 14K and superconductivity in coincidence with AF-order below 2K. The crystal structure of this hcp-compound is displayed in Figure 2.3. Various interstitial sites, called b, f, h, m, o in Wyckhoff notation, are indicated. The b- and h-sites are magnetically unique while the f-,o- and m-sites separate into up to three

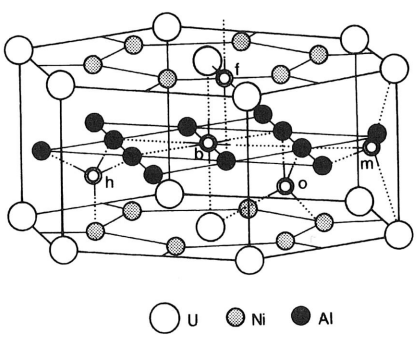

Figure 2.3. *Crystal structure of hcp UPd_2Al_3.*

magnetically inequivalent subsites, reflecting the 3-fold symmetry around the hexagonal c-axis. Identifying the x, y and z-axes of a Cartesian coordinate system with the crystalline a, b^* and c-axis, respectively, we calculate, by performing the proper lattice sum, for the unique b-site $(0, 0, \frac{1}{2})$

$$\underline{\mathbf{A}}^{\mathrm{D}}_{(b)} = \begin{pmatrix} -1.94 & 0 & 0 \\ 0 & -1.94 & 0 \\ 0 & 0 & 3.88 \end{pmatrix} \quad (kG/\mu_B)$$

and for the three inequivalent f-sites at $(\frac{1}{2}\ 0\ 0)$, $(0\ \frac{1}{2}\ 0)$ and $(\frac{1}{2}\ \frac{1}{2}\ 0)$

$$\underset{(\frac{1}{2}\ 0\ 0)}{\underline{\mathbf{A}}^{\mathrm{D}}_{(f)}} = \begin{pmatrix} 1.654 & 0 & 0 \\ 0 & -0.807 & 0 \\ 0 & 0 & -0.847 \end{pmatrix} \quad (kG/\mu_B)$$

$$\underset{(0\ \frac{1}{2}\ 0)}{\underline{\mathbf{A}}^{\mathrm{D}}_{(f)}} = \begin{pmatrix} -0.192 & -1.066 & 0 \\ -1.066 & 1.039 & 0 \\ 0 & 0 & -0.847 \end{pmatrix} \quad (kG/\mu_B)$$

$$\underset{(\frac{1}{2}\ \frac{1}{2}\ 0)}{\underline{\mathbf{A}}^{\mathrm{D}}_{(f)}} = \begin{pmatrix} -0.192 & 1.066 & 0 \\ 1.066 & 1.039 & 0 \\ 0 & 0 & -0.847 \end{pmatrix} \quad (kG/\mu_B)$$

The three $\underline{\mathbf{A}}^{\mathrm{D}}$ transform into each other by rotations of 60^0 around the c-axis. Inserting the $\underline{\mathbf{A}}^{\mathrm{D}}$ into Equation 2.70 and taking into account that for UPd_2Al_3 the susceptibility shows an axial anisotropy ($\chi_{\parallel} \neq \chi_{\perp}$) we predict for the b-site a unique angular dependence given by Equation 2.62 and no anisotropy in the basal plane (see Figure 2.4). In contrast for the f-site we predict the appearance of up to three signals, showing an anisotropy in the basal plane as well as with respect to the c-axis. E.g., choosing the b^*-axis as the axis of rotation with respect to the external field $\mathbf{H}$ (in which case we have two inequivalent subsites with relative weights of $2:1, \varphi = 0$) we obtain from Equation 2.70

$$K^{\mathrm{D}}(\theta) = A_{aa}\chi_{\perp} + (A_{cc}\chi_{\perp} - A_{aa}\chi_{\perp})\cos^2\theta + \frac{1}{2}A_{ac}(\chi_{\perp} + \chi_{\parallel})\sin^2\theta \tag{2.71}$$

If we rotate $\mathbf{H}$ in the basal plane ($\theta = 0$), we have instead

$$\begin{aligned} K^{\mathrm{D}}(\varphi) &= \left(A_{b^*b^*} + (A_{aa} - A_{b^*b^*})\cos^2\varphi + A_{ab^*}\sin 2\varphi\right)\chi_{\perp} \\ &= (A_{aa} - A_{b^*b^*}) + \sqrt{A^2_{ab^*} + (1/4)(A_{aa} - A_{b^*b^*})^2}\cos 2(\varphi - \varphi_0), \\ \tan 2\varphi_0 &= \frac{2A_{ab^*}}{A_{aa} + A_{b^*b^*}}. \end{aligned} \tag{2.72}$$

Because for the f-site $A_{ac} = 0, K(\theta)$ will show an extremum for $H \| c$-axis. This is not the case for the o-site, for example.

In the basal plane the three $K^{\mathrm{D}}(\varphi)$ curves are indeed shifted by 60^0 with respect to each other:

$$\tan 2\varphi = \pm\frac{2 \times 1.066}{0.192 + 1.039} = \pm 1.732, \qquad \varphi = \pm 60^{\circ}.$$

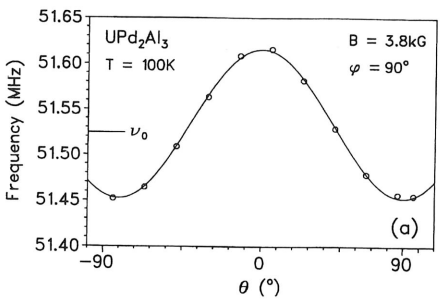

Figure 2.4. *Measured angular dependence of K in UPd_2Al_3, rotating H_{ext} in the $(b^* - c)$ plane. (Feyerherm, 1995; see also Amato, 1997).*

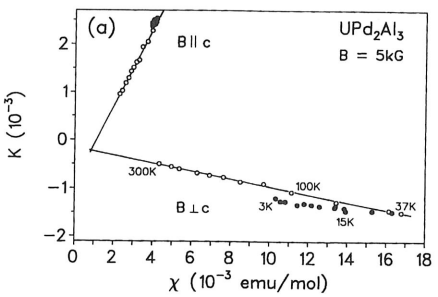

Figure 2.5. *Knight shift versus susceptibility for $H_{ext} \| c$-axis and $H_{ext} \perp c$-axis (Feyerherm 1995).*

The measurements (Feyerherm, 1995) in UPd_2Al_3 yielded only on signal with no anisotropy in the basal plane and a $\cos^2\theta$-dependence when **H** was rotated in the b^*–c-plane (see Figure 2.4). This result rules out the f-, o- and m-sites, but it is not sufficient to decide whether the b- or h-site is occupied. To settle that question one has to measure K as a function of temperature along the principle axes of the susceptibility tensor, *e.g.* for $H \| c$-axis one expects (we now have to include also the contact hf-contribution)

$$K_{\|}(T) = (A_c + A^{\mathrm{D}}_{cc})\chi_{\|}(T) \tag{2.73}$$

and for $H \perp c$-axis

$$K_{\perp}(T) = (A_c + A^{\mathrm{D}}_{aa})\chi_{\perp}(T) = (A_c - \frac{1}{2}A^{\mathrm{D}}_{cc})\chi_{\perp}(T) \tag{2.74}$$

because of $\mathrm{Tr}(\underline{\mathbf{A}}^{\mathrm{D}}) = 0$ and $A^{\mathrm{D}}_{aa} = A^{\mathrm{D}}_{b^*b^*}$. The hf-coupling constants are then obtained from the slopes of $K(T)$ versus $\chi(T)$. Figure 2.5 shows corresponding results for UPd_2Al_3. One observes indeed a linear scaling of K with χ. The analysis yields $A^{\mathrm{D}}_{cc} = +3.3kG/\mu_B$ which has to be compared with calculated values of $+3.88kG/\mu_B$ for the b-site and $-0.123kG/\mu_B$ for the h-site. We conclude that the b-site is occupied by the μ^+. The difference between the measured and calculated values is ascribed to lattice relaxation, *i.e.* an outward displacement of the two nearest U-neighbours by $\sim 5\%$.

The second example is $PrNi_5$. It has the same *hcp*-structure as UPd_2Al_3. But the μ^+ is taking a different site in this compound (Feyerherm *et al.*, 1995). This follows immediately from the observed angular dependencies, displayed in Figure 2.6. Turning the sample around the b^*-axis, *i.e.* rotating **H** in the a–c plane, we find two signals with an amplitude ratio of 1:2. Rotating H in the basal plane we find in general three signals with equal amplitudes and shifted by 60^0 with respect to each other. This looks like the f-site is involved (Figure2.6b). From the slopes of K_i versus χ_i $(i = a, b^*, c)$, restricted to $T > 80$K (why - we will discuss later), follows that $A^{\mathrm{D}}_{aa} = 1.51\mathrm{kG}/\mu_B$, $A^{\mathrm{D}}_{b^*b^*} = -0.92\mathrm{kG}/\mu_B$ and $A^{\mathrm{D}}_{cc} = -0.59\mathrm{kG}/\mu_B$ which has to be compared with calculated values of $A^{\mathrm{D}}_{aa} = 2.11\mathrm{kG}/\mu_B$, $A^{\mathrm{D}}_{b^*b^*} = -1.02\mathrm{kG}/\mu_B$ and $A^{\mathrm{D}}_{cc} = -1.09\mathrm{kG}/\mu_B$ for the f-site. The agreement is clearly bad. But there is another site, labelled i, just above or below

Figure 2.6. *Measu… a – c plane and (b) … amplitude ratio of 1:2, … (Feyerherm et al. 19…*

Figure 2.7. *L…*

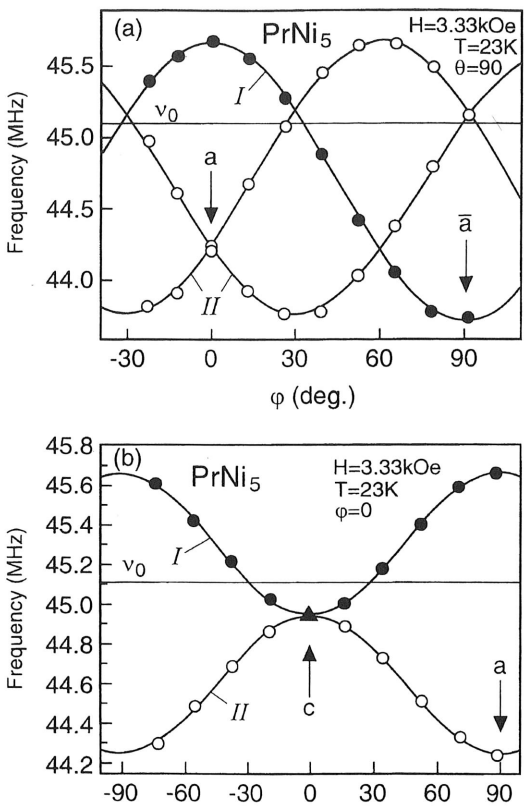

Figure 2.6. *Measured angular dependence of K in $PrNi_5$ by rotating H_{ext} in (a) the $a-c$ plane and (b) in the basal plane. In the first case two signals are seen with an amplitude ratio of 1:2, in the second case three signals with equal amplitudes can be resolved (Feyerherm et al. 1995) .*

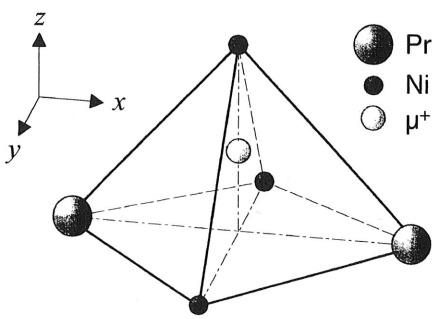

Figure 2.7. *Local atomic arrangement around the f- and i-site in $PrNi_5$.*

of the f-site as depicted in Figure 2.7. Shifting the μ^+ by ~ 0.9 Å away from the f-site perfect agreement with the calculated A_{ii}^{D} is reached. The i-site seems to be also occupied by deuterium in the compound $LaNi_5D_3$ (Hayakawa *et al.*, 1988).

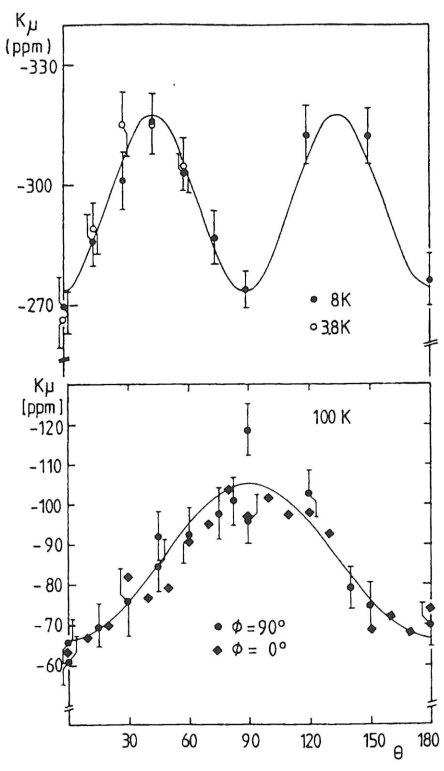

Figure 2.8. *Angular dependence of K in Bi, rotating H_{ext} in the $a-c$ plane, (a) at 8K and (b) at 100K. (Gygax et al. 1986, Baumann et al., 1986).*

2.4 A longstanding puzzle: Bi

The derivation of Equations 2.60, 2.68 or 2.70 shows that the general orientational dependence of $K(\theta, \varphi)$ is restricted to second order in the direction cosines of $\mathbf{H}$ with respect to the crystal axes irrespective of the symmetry properties and the anisotropy of χ. This is generally also observed in the experiments (preceding section). There is one notable exception, concerning the angular dependence of K in the semimetal Bi below 12K (Gygax *et al.* 1986, Baumann et al., 1986). The crystal structure of Bi can be viewed as a simple cubic lattice distorted along the body diagonal to yield a rhombohedral structure. Two interstitial sites are available in this structure. Figure 2.8 displays the angular dependence of $K(\theta, \varphi = 0)$ at 8K and at 100K. At 100K the by now familiar $\cos^2\theta$-dependence is clearly present but at 8K the angular dependence is now dominated by a $\cos^4\theta$ term,

totally unexpected vis-a-vis Equation 2.70 and not understood so far. Such behavior cannot result from the superposition of $\cos^2(\theta + \theta_0)$ terms with different θ_0.

Symmetry considerations do not forbid in principle the appearance of higher order terms in the direction cosines. In fact Boon (1964), Rubens et.al, (1973) and Weinert and Schumacher (1968) have predicted fourth order contributions as a result of an anisotropic g-factor and spin-orbit coupling which should be even visible in cubic systems. However, the predicted effects are tiny and attempts to measure them by NMR have lead to no clear evidence. Hence the μSR-results in Bi are rather singular and remain an unsolved and challenging problem.

2.5 RKKY-exchange and the contact term of the Knight shift

So far we have dealt mainly with the anisotropic aspects of the μ^+-Knight shift as introduced by the dipolar contribution. What can be learned from the other important contribution, the contact hyperfine field or the local spin density at the μ^+? As already mentioned in Section 2.2.3 measurements of K_s, which is isotropic to the extend that the conduction electron susceptibility is isotropic, in simple metals have mainly served to learn about the local electron distribution around the μ^+ formed in response to the presence of the strong Coulomb potential of the μ^+ (Schenck, 1981). In transition metal compounds, in particular in rare earth and actinide based intermetallics which contain local moments, the spin density at the μ^+ is not only a local feature but is affected by the local moments in the vicinity of the μ^+ via the RKKY-mechanism as discussed in Section 2.1.6. In this case the total contact term of the Knight shift is given by Equations 2.65, 2.66, treating the conduction electrons as a free electron gas. Since the induced spin polarisation of the conduction electrons decays with the inverse third power of the distance from a local moment, *e.g.* an f-electron atom (see Equation 2.36), we assume that only the nearest local moment neighbours affect the spin density at the μ^+. Recalling that the Pauli spin susceptibility is temperature independent, while the susceptibility associated with the local moments, *e.g.* of the f-electrons, is strongly temperature dependent we may rewrite Equation 2.65 in the following condensed form

$$K_f(T) = K_0 + A_f \chi_f(T) \tag{2.75}$$

where $A_f \propto J$ (see Equation 2.66).

From measurements of the slope of $K_f(T)$ versus $\chi_f(T)$ it should be possible to deduce some information on the exchange parameter (exchange integral). J is a very important parameter which not only enters into the RKKY-interaction but also determines the strength of the on-site Kondo screening. The Kondo temperature T_K depends on J as follows

$$T_K \propto \frac{1}{k_B} \exp\left(\frac{1}{JN(\varepsilon_F)}\right), \tag{2.76}$$

where $N(\epsilon_F)$ is the density of states at the Fermi energy. The RKKY-interaction, on the other hand, is responsible for the inter-site coupling of the local moments which may lead to magnetic order. The ordering temperature follows

$$T_{\mathrm{RKKY}} \propto \frac{1}{k_B} J^2 N(\varepsilon_F). \tag{2.77}$$

The on-site Kondo effect tries to form a nonmagnetic spin singlet state, while the inter-site RKKY-interaction tries to establish magnetic order, usually of an antiferromagnetic type. Figure 2.9 shows in a schematic way the dependence of T_K and T_{RKKY} on J. (Doniach's phase diagram; Doniach, 1977). In the region where $T_K \gg T_{\mathrm{RKKY}}$ nonmagnetic behavior should prevail, while for $T_{\mathrm{RKKY}} \gg T_K$ magnetic order is expected. The so called heavy fermion systems are characterised by comparable T_K and T_{RKKY}, *i.e.* the two mechanism are roughly of similar strength. As a consequence the ground state properties of heavy fermion systems turn out to be rather complex.

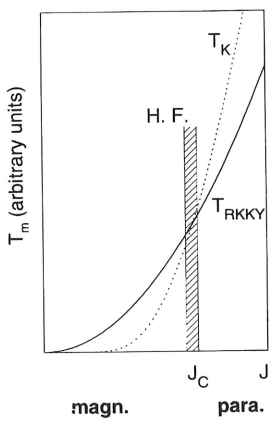

Figure 2.9. *Schematic view of the dependence of T_K and T_{RKKY} on the exchange parameter J (Doniach's phase diagram).*

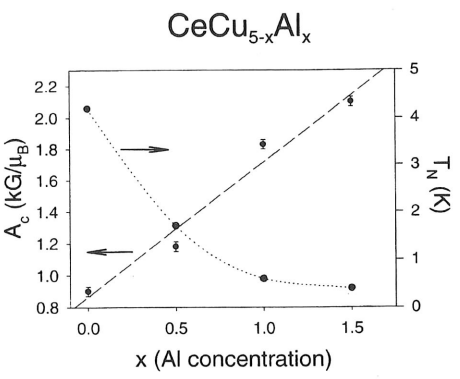

Figure 2.10. *Contact coupling constant A_f in $CeCu_{5-x}Al_x$ versus x (A Amato on the basis of Wiesinger et al., 1997).*

An interesting system in which to study the correlation of magnetic order and the parameter J is $CeCu_{5-x}Al_x$. Pure $CeCu_5$ displays long range local moment magnetic order with $T_N \simeq 4.1$K, $CeCu_3Al_2$ on the other hand is nonmagnetic with a Kondo temperature of $T_K \simeq 9.5$K. For $x \leq 1.5$ ZF-μSR measurements have revealed spin glass like behavior with the spin-glass freezing temperature decreasing with increasing x (Wiesinger *et al.*, 1995). Hence we expect that the parameter J should increase with x. This is clearly confirmed by μ^+ Knight shift measurements on polycrystalline samples (Wiesinger *et al.*, 1997). Figure 2.10 shows a plot of A_f, deduced from the slope of $K_f(T)$ versus $\chi_f(T)$, as a function of x. Since $A_f \propto J$ we conclude that $J \propto x$. There may be two reasons why J rises with x: (i) replacing monovalent Cu by trivalent Al enhances the number of conduction electrons and (ii) the substitution leads to an increase of the c/a-ratio. Both effects may enhance the hybridisation of the local f-electron state and the delocalised conduction electrons thereby increasing J.

2.6 μ^+-Knight shift in type II superconductors

The measurement of the μ^+ Knight shift in the superconducting state of type II-superconductor above H_{c1} is made difficult by the onset of diamagnetism below T_c which

usually is causing a shift which is much larger (and negative) than the μ^+ Knight shift in nontransition metals (this is in contrast to the nuclear Knight shift). Chances to observe something like the Yosida curve (see Section 2.1.5) are therefore much higher in transition metal compounds where, moreover, pinning of vortices may suppress the development of diamagnetism below T_c.

The appearance of the vortex lattice below T_c leads to a further complication which arises from the inhomogeneity of the distribution of paired and unpaired electrons. In the center core of a vortex the electrons are unpaired and respond to the applied field as in the nonsuperconducting phase, while outside of the core the density of Cooper pairs rises to its maximum within a distance of a few coherence length ξ and the magnetic response will be modified depending on the symmetry of the superconducting state. The ratio of core volume to the inter vortex volume depends on the density of the flux lines and is roughly given by

$$\frac{V_{\rm c}}{V_{\rm c}+V_{\rm ic}} \simeq \frac{B}{B_{\rm c2}(T)}. \tag{2.78}$$

The inhomogeneity in the distribution of paired and unpaired electrons will lead to a corresponding inhomogeneity in the Knight shift distribution. In a simple model the distribution may be approximated by two values; in the core region by the Knight shift observed also above T_c and elsewhere by some average modified value. The μSR-signal is then expressed as

$$P(t) = a_{\rm c}\cos(\omega_{\rm c}t) + a_{\rm ic}\exp\left(-\frac{1}{2}\sigma^2t^2\right)\cos\left(\omega_{\rm ic}t\right) \tag{2.79}$$

with

$$\frac{a_{\rm c}}{a_{\rm c}+a_{\rm ic}} = \frac{V_{\rm c}}{V_{\rm c}+V_{\rm ic}} = \frac{B}{B_{\rm c2}(T)}. \tag{2.80}$$

The Gaussian damping factor accounts for the inhomogeneous field distribution in the intervortex space and depends on the London magnetic penetration depth.

It proved that such a two component approach was absolutely necessary in order to obtain meaningful results from Knight shift measurements in the superconducting state of the already discussed UPd_2Al_3 (Feyerherm et al., 1994). (see Section 2.6). Remember that the superconducting state coexists with AF-magnetic order. The reason that in this state the Knight shift could be measured at all rests in the lucky circumstance that the μ^+ resides at the b-site (see Section 2.6), where due to the high symmetry of this site the fields arising from the ordered moments cancel rather precisely (see also Section 3.1). Figure 2.11 displays the temperature dependence of the relative shift of $\omega_{\rm ic}$ below 2.5K for two different orientations of the applied field $\mathbf{H}$; $\omega_{\rm c}$ was kept at the average of the displayed values above T_c. For the following discussion we reproduce here once more the Equations 2.73 and 2.74

$$\begin{aligned} K_{\parallel}(T) &= (A_c + A_{cc}^{\rm D})\chi_{5f,\parallel}(T), \\ K_{\perp}(T) &= (A_c - \frac{1}{2}A_{cc}^{\rm D})\chi_{5f,\perp}(T). \end{aligned}$$

What can we learn from these results?

(i) $A_{cc}^{\rm D}$ and A_c were determined already from the slopes of $K_i(T)$ versus $\chi_i(T)$ at higher temperatures. Assuming that these parameters (certainly $A_{cc}^{\rm D}$) are temperature

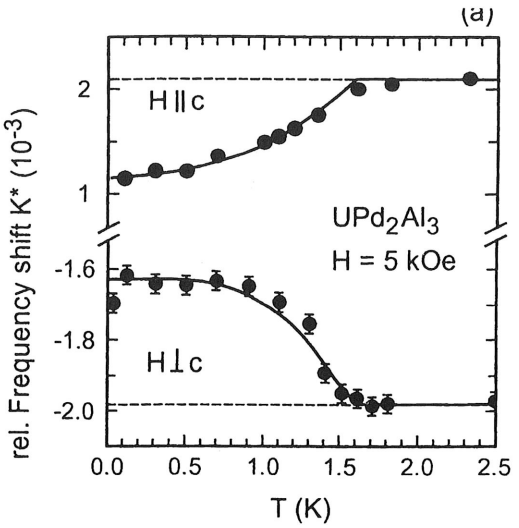

Figure 2.11. *μ^+-Knight shift in UPd_2Al_3 for $H_{ext}\|c$-axis and $H_{ext}\perp c$-axis in the superconducting range.*

independent the observed decrease in absolute value of the frequency shifts reflects directly a decrease of $\chi_{5f,i}(T)$. If, on the other hand, A_c had changed below T_c it would have affected $K_{\|}(t)$ and $K_{\perp}(T)$ differently, *e.g.* a drop in A_c would have reduced $K_{\|}$ and would have increased the absolute value of $K_{\perp}$ in contrast to what is observed. Hence we conclude that the Knight shift behavior reflects directly the susceptibility $\chi_{5f}(T)$.

(ii) The change of $\chi_{5f,\|}(T)$ and $\chi_{5f,\perp}(T)$ below T_c turns out to be isotropic in sharp contrast to the anisotropy of the total susceptibility. This suggest that the total susceptibility consist of two contributions, an isotropic term and an anisotropic one:

$$\underline{\boldsymbol{\chi}}_{5f}(T) = \chi_i(T)\underline{\mathbf{E}} + \underline{\boldsymbol{\chi}}_{5f,\mathrm{an}}(t) \tag{2.81}$$

This idea leads further to the suggestion that in fact two different electron states are involved: $\chi_i(T)$ which reflects the onset of superconductivity is associated with the heavy quasiparticles which condense into Cooper pairs below T_c; $\underline{\boldsymbol{\chi}}_{5f,\mathrm{an}}$ is associated with the $5f$-electron subsystem which is responsible for the local moment antiferromagnetism (Feyerherm *et al.*, 1994). This conjecture of two rather independent $5f$-substates is supported by other observations and seems to hold also for other U-based heavy electron compounds.

(iii) The drop of $\chi_i(T)$ below T_c points to presence of an even-parity singlet-pairing superconducting state. This is in agreement with NQR measurements of the nuclear spin lattice relaxation rate $1/T_1$ which shows a T^3 behavior which is explained in terms of a d-wave even-parity superconducting state (Kyogaku *et al.*, 1993).

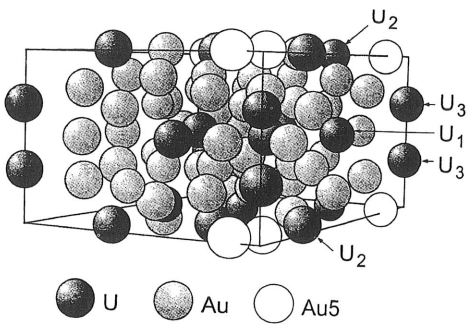

Figure 2.12. *Crystal structure of hcp* $U_{14}Au_{51}$.

2.7 Compounds with inequivalent magnetic ions

As discussed in the previous section measurements of the μ^+-Knight shift can be used to study locally the magnetic response or the magnetic susceptibility. This opens up interesting possibilities in systems containing different magnetic ions or magnetic ions in crystallographically inequivalent sites. The hope is that the μ^+ is located close enough to only one variety to be affected by its magnetic response. Conventional bulk measurements of the susceptibility only yield an average information:

$$\chi_{\text{bulk}} = \sum_i p_i \chi_i, \tag{2.82}$$

where p_i is a measure of the relative abundance of a particular magnetic atom i.

Recent Knight shift measurements in the moderately heavy fermion compound $U_{14}Au_{51}$ demonstrated indeed that the individual magnetic response of a particular magnetic atom can be monitored (Schenck *et al.*, 1998). $U_{14}Au_{51}$ is a hexagonal compound which undergoes a magnetic transition into a rather complex AF-magnetic state below 22K. (see Section 3.2) The U-atoms occupy three crystallographically different sites labelled as U1, U2 and U3 (s. Figure 2.12). Neutron scattering studies revealed that the ordered moments assume different values, the U3-ion showing even a zero ordered moment (Dommann *et al.*, 1990; Brown *et al.*, 1997).

TF-μSR measurements produced four components in the signal. One component could be ascribed to μ^+ sitting near the $(0\ 0\ \frac{1}{2})$ site, *i.e.* half way between two U3-ions, the other three components are associated with a site at three magnetically equivalent positions in the $(0\ 0\ \frac{1}{2})$-plane inside a triangle formed by U1-ions. The first component revealed that also in the paramagnetic state the magnetic response of the U3-ions is much reduced, but not zero. The three other components showed Knight shifts which were well described by a Curie-Weiss behavior, *i.e.*

$$K_i = K_{0,i} + A_i \frac{C}{T - \Theta}, \tag{2.83}$$

as displayed in Figure 2.13. The plot reveals Curie-Weiss temperatures which are rather different from those characterising the bulk magnetic susceptibility, showing even an anisotropy in the basal plane. These must be associated with the magnetic response of the U1-ions, since the U2-ions in the $(0\ 0\ 0)$-plane are too far away to contribute noticeably to the local fields at the μ^+. Figure 2.13 relates to one of the three inequivalent

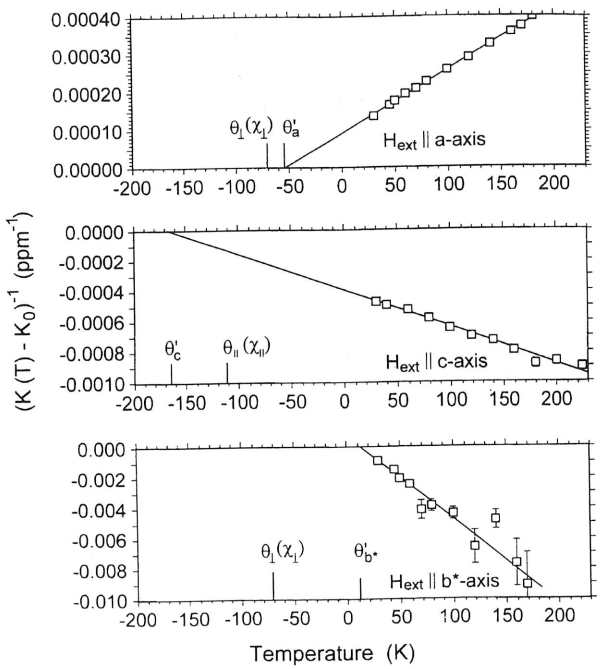

Figure 2.13. *Curie-Weiss plot of* $(K_i(T) - K_0)^{-1}$ *versus temperature. Note the shifted positions of the Curie-Weiss temperatures* θ_i' *with respect to the bulk* $\theta_\perp$ *and* $\theta_\parallel$ *(Schenck et al., 1998).*

sites. For the other two sites the axis-assignments in the basal plane have to be changed to $H_{\rm ext}\|b$-axis or $H_{\rm ext}\|a*$-axis in the upper graph and to $\mathbf{H}_{\rm ext}\|a*$-axis or $H_{\rm ext}\|b$-axis in the lower graph. The average local susceptibility over all three sites, corresponding to the bulk average, is then given by

$$\begin{aligned}\chi_\perp(U1) &= \frac{1}{3}\left(\chi_a(U1) + 2\chi_{b*}(U1)\right) \\ &= \frac{C}{3}\left(\frac{1}{T-\theta_a'} + \frac{2}{T-\theta_{b*}'}\right)\end{aligned}$$

which, for $T > 0$ ($\theta_i' < 0$), can be approximated by

$$\chi_\perp(U1) \simeq \frac{C}{T - (\theta_a' + 2\theta_{b*}')/3}$$

with $\theta_\perp(U1) = (\theta_a' + 2\theta_{b*}')/3 = -10$K.

This new average value is still quite different from the –72K following from $\chi_{\perp,\rm bulk}$, but we have not yet taken into account that there will be also a contribution from the U2-ions. So we postulate

$$\chi_\perp(U_1 + U_2) = \frac{1}{2}\left(\chi_\perp(U1) + \chi_\perp(U2)\right)$$

and

$$\theta_{\perp}(U1+U2) = -72 \cong (-10 + \theta_{\perp}(U2))\,\frac{1}{2}$$

or

$$\theta_{\perp}(U2) \simeq -132\text{K} \ .$$

Correspondingly we obtain

$$\theta_{\parallel}(U2) \cong -58\text{K} \ .$$

Neutron scattering has been used to measure the induced moments on the U1- and U2-sites at 22K in an applied field of 4.6T parallel to the c-axis with the result: $\mu(U1) = 0.05\mu_B$ and $\mu(U2) = 0.10\mu_B$ (Brown *et al.*, 1997) or $\mu(U1)/\mu(U2) = 0.5$. Assuming that the Curie constant C is isotropic we calculate with the above estimated Curie-Weiss temperatures

$$\frac{\mu(U1)}{\mu(U2)} = \frac{22+58}{22+164} \simeq 0.43$$

which is in good agreement with the neutron result.

2.8 μ^+-induced modification of local magnetic susceptibility

By implanting a positive muon into a metal matrix one adds a strong Coulomb potential to the otherwise periodic crystal potential which, at least locally, should cause a severe disturbance. It can be expected that this disturbance will also lead to changes in the local magnetic response as compared to the undisturbed case. So far, however, we have not encountered any real evidence for such modifications. This is not because such modifications do not exist but rather due to my choice of examples so far.

Let me first present an example where the induced modifications by the μ^+ are well understood. Figure 2.14 displays a plot of the μ^+ Knight shift K_i and the bulk magnetic susceptibility χ_i (normalised to the Knight shift at the highest temperature) in $PrNi_5$ for different orientations i. (Feyerherm *et al.*, 1995). We see that above $\sim$ 80K K_i scales well with χ_i so that the Equations 2.73 and 2.74 will hold. This allowed to determine the μ^+-position as discussed in Section 2.3. Below 80K we notice a severe deviation from a scaling behavior. Even a change in sign is found for one of the two signals for $H\|a$-axis. How can this be understood? Of course, one suspects that the magnetic response of most likely only the nearest Pr^{3+}-neighbours (for the i-site there are two) are modified, while all more distant Pr^{3+}-ions remain unaffected by the presence of the μ^+. Equations 2.73 and 2.74 may then be split into two contributions, arising from the nearest neighbours (nn) and the rest, which exhibit an unchanged magnetic response

$$\begin{aligned}
K_a &= \left(A^{\mathrm{D}}_{aa,\mathrm{nn}} + A_c\right)\chi_{a,\mathrm{nn}} + A^{\mathrm{D}}_{aa,\mathrm{rest}}\chi_{\perp,\mathrm{bulk}} \\
K_{b^*} &= \left(A^{\mathrm{D}}_{b^*b^*,\mathrm{nn}} + A_c\right)\chi_{b^*,\mathrm{nn}} + A^{\mathrm{D}}_{b^*b^*,\mathrm{rest}}\chi_{\perp,\mathrm{bulk}} \\
K_c &= \left(A^{\mathrm{D}}_{cc,\mathrm{nn}} + A_c\right)\chi_{c,\mathrm{nn}} + A^{\mathrm{D}}_{cc,\mathrm{rest}}\chi_{\parallel,\mathrm{bulk}}
\end{aligned}$$

It is also assumed that the contact contribution arises dominantly only from the nearest neighbours. Since the μ^+-site is known $\underline{\mathbf{A}}^{\mathrm{D}}_{(\mathrm{nn})}$ and $\underline{\mathbf{A}}^{\mathrm{D}}_{\mathrm{rest}}$ can be calculated. Also A_c is known from the scaling behavior above 80K. This allows us now to extract the local susceptibility $\underline{\boldsymbol{\chi}}_{(\mathrm{nn})}(T)$ associated with the two nearest neighbours. $\underline{\boldsymbol{\chi}}_{(\mathrm{nn})}(T)$ is displayed

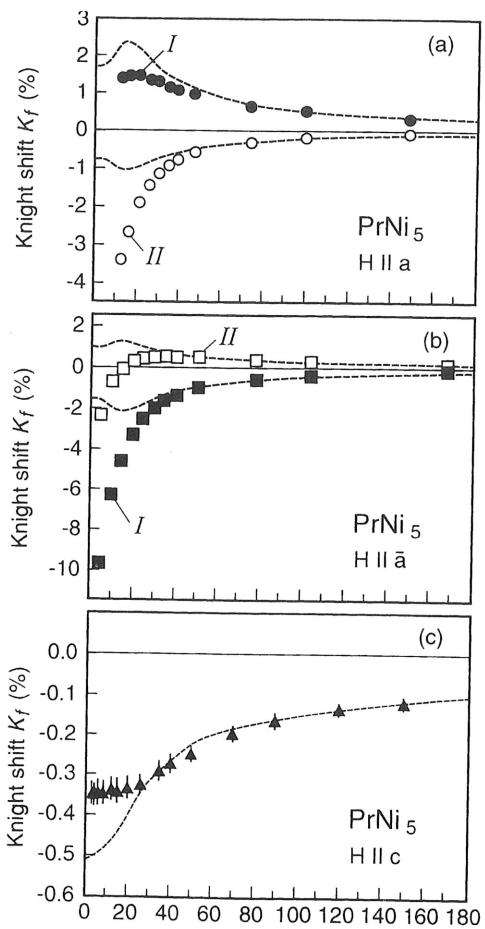

Figure 2.14. *Temperature dependence of K_i and bulk susceptibility χ_i in $PrNi_5$. χ_i is normalised to K_i at the highest temperature (Feyerherm et al., 1995).*

in Figure 2.15. We notice that the local susceptibility is also anisotropic in the basal plane. The principal axes x, y of $\underline{\chi}_{(\mathrm{nn})}$ in the basal plane are along the lines connecting the two nearest Pr^{3+}-neighbours (x) and the two nearest Ni-neighbours (y), respectively (see Figure 2.7). The presence of the μ^+ will in two ways affect a nn Pr^{3+}-ion: (i) the local point symmetry of that site will be changed, (ii) the screened μ^+-charge will produce some additional electric field at the Pr^{3+}-ion. We must pay attention to the fact that the magnetic properties of the Pr^{3+}-ion are primarily associated with the crystalline electric field (CEF) splitting of $^3H_4$-ground state multiplet of the $4f^2$-configuration of Pr^{3+}. The CEF-splitting of Pr^{3+} in $PrNi_5$ is well known from inelastic neutron scattering work (*e.g.* Amato et al., 1992). The ground state level is a non magnetic singlet (Γ_4) state as is the first excited state (Γ_1) 23K above the Γ_4-state (see Figure 2.16). The effect of the μ^+ will be that the symmetry of the CEF-Hamiltonian will be changed as well as the strength of

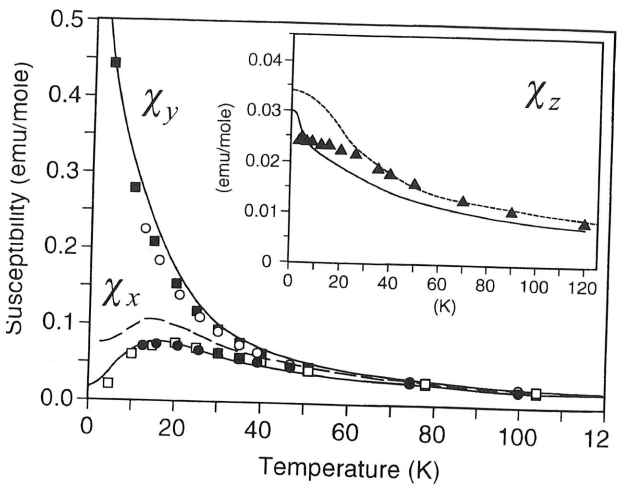

Figure 2.15. *Temperature dependence of the modified local susceptibility associated with the two nearest Pr-neighbours (Feyerherm et al., 1995).*

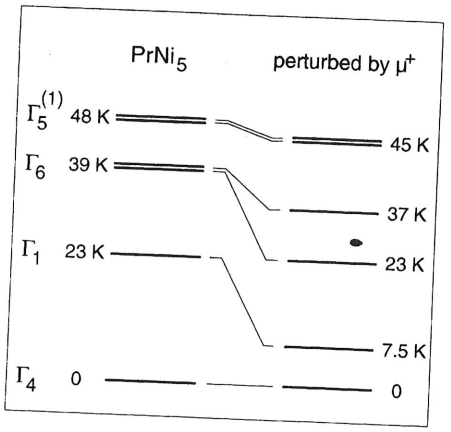

Figure 2.16. *CEF-splitting with and without the μ^+ of the $^3H_4$ groundstate multiplet of $PrNi_5$ (Feyerherm et al., 1995).*

CEF-potential. In the undisturbed case the hexagonal CEF Hamiltonian reads

$$\mathcal{H}_{\mathrm{CEF}} = B_2^0 0_2^0 + B_4^0 0_4^0 + B_6^0 0_6^0 + B_6^6 0_6^6, \tag{2.84}$$

where the B_ℓ^m and 0_ℓ^m (Stevens operators) are defined as usual. The lowering of the symmetry will cause additional terms $B_\ell^m 0_\ell^m$ to appear in Equation 2.84. The magnetic susceptibility for a CEF-split groundstate multiplet can be calculated with Equation 2.23 which requires the determination of the eigenvalues and eigenstates of the CEF-Hamiltonian.

Admitting an additional term $B_2^2 0_2^2$ and allowing B_2^0 and B_2^2 to vary independently χ_{CEF} was calculated and fitted to data shown in Figure 2.15. Best fits are indicated by the solid lines. The resulting modified CEF-level scheme of the nearest Pr^{3+} are also displayed in Figure 2.16. Below we compare the fitted B_2^m values with undisturbed ones

	no μ^+	with μ^+
B_2^0(eV)	0.51(1)	0.555(5)
B_2^2(eV)	0	+0.085(5)

All other B_ℓ^m, which are quite small, remain unchanged. The modified local susceptibility can thus completely be accounted for by a modified CEF-interaction, modified due to the presence of the μ^+. However, it was not possible to reproduce the new B_2^m by a simple point charge model.

In the presented case it was possible to rationalise the μ^+-induced modifications of the local susceptibility, but there are other examples where we do not yet understand the μ^+-induced effects. A striking example is provided by measurements in the heavy fermion compound URu_2Si_2. Figure 2.17 shows again a plot of K versus χ_{5f}. Above 60K K scales with χ_{5f} but below 60K K becomes essentially temperature independent while $\chi_{5f,\|}$ shows a maximum near 50K and drops by almost 50% when lowering the temperature to $\sim$ 10K.

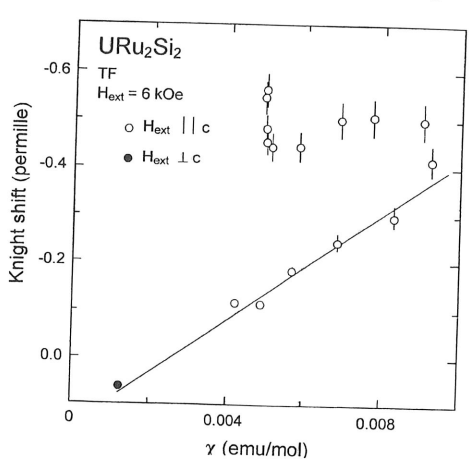

Figure 2.17. *μ^+-Knight shift in URu_2Si_2 versus bulk susceptibility (Knetsch et al., 1993).*

2.9 Transitions between different valence configurations

Mixed valent, intermediate valent and valent transitions are not uncommon in rare earth intermetallic compounds. E.g. Ce may appear as a Ce^{2+}-ion with one $4f$-electron in the $4f$-shell that renders it magnetic, or as a Ce^{3+}-ion where the f-electron has become a delocalised conduction electron and consequently nonmagnetic. Valent transitions may be accompanied by metal-insulator or metal-semiconductor transitions. μSR-spectroscopy has not been applied very systematically to the study of such phenomena. In fact I know of only one good example which, nonetheless, demonstrates that much could be gained from such studies. The example concerns the cubic pseudo-binary systems $Sm_{0.9}La_{0.1}S$ and

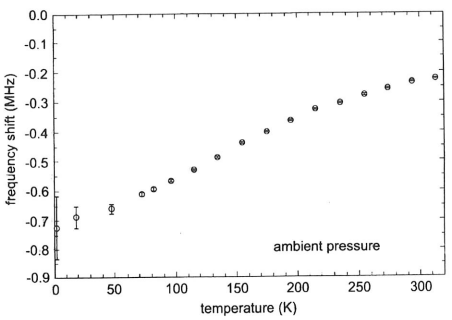

Figure 2.18. *Temperature dependence of the frequency shift* $(\nu(T)\_\nu_0)$ *in* $Sm_{0.85}Tm_{0.15}S$ *at ambient pressure).*

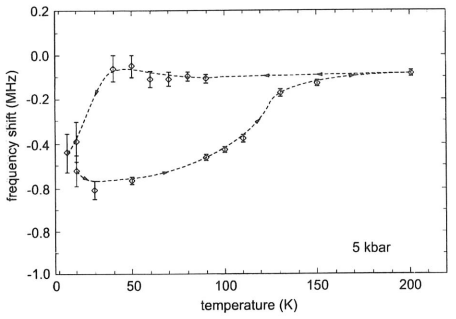

Figure 2.19. *Temperature dependence of the frequency-shift at 5kbar. (Both figures are unpublished data, PSI 1996).*

$Sm_{0.85}Tm_{0.15}S$. The motivation for looking at these systems is based on the hypothesis that if the system is exposed to above a certain critical pressure a condensed exitonic state is formed. The idea is that the strong Coulomb interaction between $4f$-holes and conduction electrons produces exitons that condense into a new type of ground state (Wachter *et al.*, 1995) that is supposed to be nonmagnetic and insulating. At ambient pressure the systems are metallic, exhibiting an intermediate valence and they become indeed insulators above a certain critical pressure and at low temperatures. What could not be checked was the loss of paramagnetism and here it was thought that μSR via Knight shift measurements could help out. Since SmS is a cubic system (NaCl) and the only interstitial site possesses a cubic point symmetry as well, the only contribution to the μ^+-Knight shift will be the contact hyperfine field. Figure 2.18 shows the temperature dependence of the frequency shift $\nu(T) - \nu_0$ ($\nu_0 = \gamma_\mu H_{\text{ext}}$) in $Sm_{0.85}Tm_{0.15}S$ at ambient pressure ($H_{\text{ext}} = 6$kOe). It reflects the behavior of the magnetic susceptibility in SmS (apparently the Tm contribution is not seen). Figure 2.19 shows the temperature dependence of the frequency shift at a pressure of 5kbar. A strongly hysteretic behavior shows up. The same is observed as a function of pressure at 80K (Figure 2.20). Compared to Figure 2.18 it is seen that the frequency shift (Knight shift) is much reduced and essentially temperature independent above a pressure dependent critical temperature. Before discussing this, it needs to be mentioned that, well separated from the μSR signal from the sample, one could also see the signal from the μ^+ stopping in the walls of the Ti-pressure cell. The temperature dependence of the corresponding frequency shift is displayed in Figure 2.21 It reflects the bulk magnetisation of the sample which produces an additional field in its environment. We see that the shift is pressure independent. Moreover it displays the same temperature dependence as the susceptibility of the sample at ambient pressure. The conclusion is that the paramagnetic response of the sample does not collapse as the pressure is raised above a certain critical value.

Also the collapse of the μ^+-Knight shift under pressure and at high temperature is not related to the formation of the exitonic condensed state. It rather reflects the well known 1st-order transition from an intermediate valent to a trivalent state. However, the collapse of the μ^+-Knight shift and its temperature independence is quite puzzling.

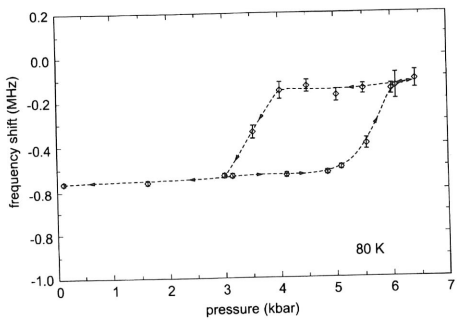

Figure 2.20. *Pressure dependence of the frequency shift at 80K. (Both figures are unpublished data, PSI 1996).*

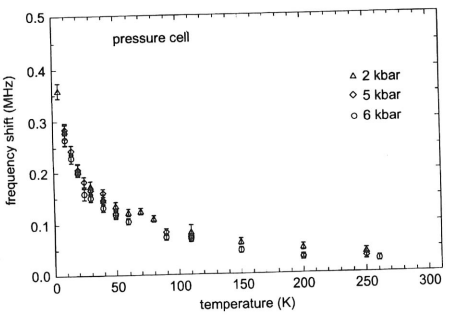

Figure 2.21. *Temperature dependence of the frequency shift of μ^+ stopping in the walls of the pressure cell.*

It implies that either the local susceptibility is suppressed and has become temperature independent or that the coupling constant $A_{c,4f}$ has dropped to a very small value and only a temperature independent term (see Equation 2.66 or 2.77) may be left. Even if μ^+-induced effects were involved they are strongly connected to the valence transition.

2.10 Paramagnetic and diamagnetic domains in Be

In Section 2.1.4 we have discussed the expected coexistence of diamagnetic and paramagnetic (Condon) domains in the de Haas-van Alphen regime of the magnetic response of conduction electrons if $4\pi\partial M/\partial B \geq 1$. Until recently the only direct evidence for this phenomenon was provided by an NMR experiment on Silver where the free induction decay in a single crystal was observed. The presence of different domains was revealed by a splitting of the NMR line (Condon and Walstedt, 1968). In principle an even better system to study the Condon domains should be *Be* but NMR measurements proved to be inconclusive, in part due to quadrupole splitting of the NMR line. Since the μ^+ is immune to quadrupolar interaction it may in fact be a better probe to study the development of the Condon domains. And indeed, this turned out to be the case (Solt *et al.*, 1996 and to be published).

Figure 2.22 shows the Fourier transform of the μSR signal from a single crystal *Be*-plate, obtained at 0.5K and $H = 20634$Oe. The field is applied parallel to the normal of the plate so that the demagnetisation factor $N \simeq 4\pi$. At this field the magnetisation $M(B)$ passes through a node. Clearly a splitting is seen which can be associated with the simultaneous presence of differently magnetised domains. According to Equation 257 the total field seen by the μ^+ is given by

$$\mathbf{B}_\mu = \mathbf{H} + \frac{4\pi}{3}\mathbf{M}_d - N\mathbf{M}_S + \mathbf{B}_{\varepsilon L} \tag{2.85}$$

Note that the Lorentz field is determined by the domain magnetisation, while the demagnetisation field depends on the effective sample magnetisation. $\mathbf{B}_{\varepsilon L}$ arises from sources inside the Lorentz sphere. In the present case, these sources are the electrons moving on

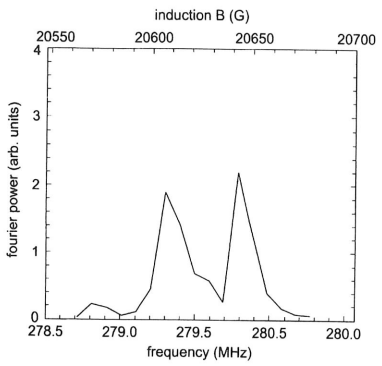

Figure 2.22. *Fourier transform of μSR signal obtained at 0.5K and H_{ext} = 20634 Oe in Be (Solt et al. 1996).*

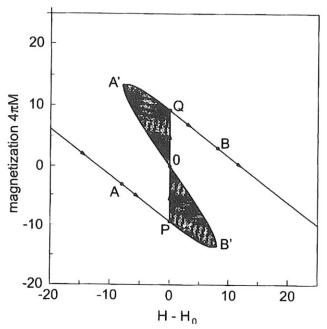

Figure 2.23. *Calculated $4\pi M$ as a function of H near a node in $M(B)$ occurring at H_0. (Solt et al. 1998.)*

Landau orbitals with cyclotron radii of several thousand Å. One can show that in this case $\mathbf{B}_{\varepsilon L} = (8\pi/3)\mathbf{M}_d$ so that

$$\mathbf{B}_\mu = \mathbf{B} = \mathbf{H} + 4\pi\mathbf{M}_d - N\mathbf{M}_S \tag{2.86}$$

Since in this experiment $N \simeq 4\pi$ there will be regions where the condition $B = H_{\text{ext}}$ can only be fulfilled if the volume splits into paramagnetic and diamagnetic domains, extending parallel to $\mathbf{H}$ through the plate, as we have seen in Section 2.1.4. Figure 2.23 displays the calculated

$4\pi M$ as a function of the applied field H in a restricted range around H_0, corresponding to a node in $M(B)$. For $H < H_0$ the sample shows a diamagnetic behavior ($4\pi M < 0$). At the point P, where $H = H_0$, the forbidden B-range is entered and paramagnetic domains with $4\pi M_Q > 0$ grow at the expense of the diamagnetic volume fraction with $4\pi M_P < 0$ until the whole volume becomes paramagnetic. Note that $|M_P| = |M_Q|$. This is nicely reflected in Figure 2.24 which shows how the splitting of the μSR-signal appears and disappears with the periodicity of the dHvA-cycle. Figure 2.25 shows the corresponding behavior of the signal amplitudes. We notice that in the split region the μ^+ sees H-independent internal inductions B_μ. This can be rationalised as follows: the constancy of M_Q and M_P in the forbidden region requires that also the effective internal field H_i is constant. H_i follows from

$$\mathbf{H}_i = \mathbf{H} - N\mathbf{M}_S = \mathbf{B}_P - 4\pi\mathbf{M}_P = \mathbf{B}_Q - 4\pi\mathbf{M}_Q = \mathbf{H}_0 \tag{2.87}$$

or

$$\mathbf{H}_i = \mathbf{H}_0 + \delta\mathbf{H} - N\mathbf{M}_S = \mathbf{H}_0 \tag{2.88}$$

or

$$N\mathbf{M}_S = \delta\mathbf{H}, \tag{2.89}$$

i.e. the deviation of H from H_0 is compensated by the change in the average sample magnetisation. Hence we rewrite Equation 2.86 as follows

$$\mathbf{B}_\mu(P,Q) = \mathbf{H}_0 + \delta\mathbf{H} + 4\pi\mathbf{M}_{P,Q} - N\mathbf{M}_S = \mathbf{H}_0 + 4\pi\mathbf{M}_{P,Q} = \text{const.} \tag{2.90}$$

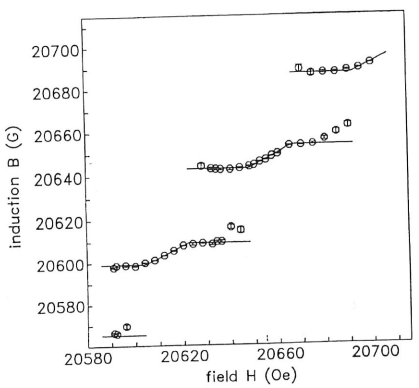

Figure 2.24. *Field dependence of the splitting of the μSR signal displaying the periodicity of the $dHvA$-cycle (both figures Solt et al. 1996, 1998)*

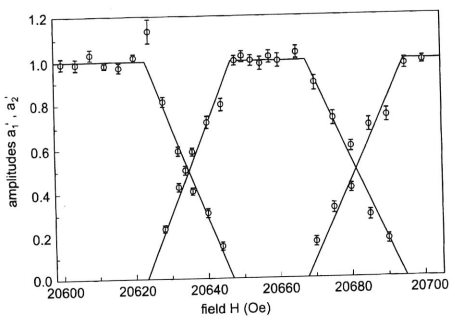

Figure 2.25. *Field dependence of the fraction of paramagnetic and diamagnetic domains (amplitudes a_1, a_2)*

According to Equation 2.33

$$M_S = (1-\alpha)M_P + \alpha M_Q \quad , \quad \alpha = \frac{v_d}{v_d + v_p}.$$

and therefore (in the forbidden range)

$$\alpha = \frac{\delta H - N M_P}{N(M_Q - M_P)} = \frac{\delta H + N|M_P|}{2N|M_P|} \tag{2.91}$$

The linear dependence of α on H is clearly visible in Figure 2.25

3 μSR-spectroscopy in magnetically ordered phases

3.1 Magnetic structure and internal field distributions

The microscopic magnetic field at the μ^+-site or sites in the magnetically ordered phase consists, as in the paramagnetic phase, of dipolar and contact hyperfine components. In the paramagnetic phase the static moments on each magnetic ion site had to be induced by an external field. The moment arrangement in this case corresponds to a ferromagnetic structure. In the ordered phase each magnetic ion at site $\mathbf{r}_i$ possesses naturally a static moment $\boldsymbol{\mu}(\mathbf{r}_i)$ and contributes to the net magnetic field at a given site ($\mathbf{r}_\mu$) which is then given by a sum over all individual sources at $\mathbf{r}_i$ (see also Equations 2.48, 2.54)

$$\mathbf{B}_\mu = \sum_i \left(\underline{\mathbf{A}}^{\mathrm{D}}(\mathbf{r}_\mu - \mathbf{r}_i) + \underline{\mathbf{E}} A_c(\mathbf{r}_\mu - \mathbf{r}_i) \right) \cdot \boldsymbol{\mu}(\mathbf{r}_i) \tag{3.1}$$

For simplicity we assume here that only one type of magnetic ion is present. Usually a fair assumption is that the contact hyperfine field at the μ^+ is caused by only its nearest

neighbours with equal distance. We may then write

$$\mathbf{B}_\mu = A_c \sum_j \boldsymbol{\mu}(\mathbf{r}_{\mathrm{nn},j}) + \sum_i \underline{\mathbf{A}}^{\mathrm{D}}(\mathbf{r}_\mu - \mathbf{r}_i) \cdot \boldsymbol{\mu}(\mathbf{r}_i) \tag{3.2}$$

As in the paramagnetic phase $\underline{\mathbf{A}}^{\mathrm{D}}(\mathbf{r}_\mu - \mathbf{r}_i)$ and the lattice sum are determined by the crystal structure and the μ^+-site or sites. A_c may be taken from measurements of the contact contribution to the Knight shift. The additional feature entering into Equation 3.2 is the moment arrangement as symbolised by $\mu(\mathbf{r}_i)$. In a ferromagnetic $\boldsymbol{\mu}$ is the same for every $\mathbf{r}_i$. In an antiferromagnet it is often convenient to characterise the magnetic structure by a propagation vector $\mathbf{k}$, so that

$$\boldsymbol{\mu}(\mathbf{r}_i) = \boldsymbol{\mu}\left(\mathbf{r}_j + \mathbf{k}(\mathbf{r}_j - \mathbf{r}_i)\right) \tag{3.3}$$

for certain $\mathbf{r}_j - \mathbf{r}_i$. More complicated structures can be described by using multiple $\mathbf{k}$-arrangements. In Equation 3.3 the vector $\mathbf{k}$ is some rational multiple of the reciprocal lattice vector $\mathbf{G}$, so that indeed the same moment direction is repeated at some distance commensurable with the lattice periodicity. In any case if $\boldsymbol{\mu}(\mathbf{r}_i)$ and the μ^+-site are known it is relatively straightforward to calculate $\mathbf{B}_\mu$ to any desired precision throughout the involved crystal. This may be done in the real lattice space or one may use Fourier transform techniques (see *e.g.* Dalmas de Reotièr and Yaouanc, 1997). In this way one finds that magnetically equivalent sites (which are of course also crystallographically equivalent) are associated with a distinct $\mathbf{B}_\mu$. If there are several magnetically inequivalent μ^+-positions more than one distinct field may be present (*e.g.* in ferromagnetic bcc-iron, where the μ^+ is supposed to be located at a tetrahedral site with two magnetically inequivalent versions two distinct fields are expected). If the propagation vector $\mathbf{k}$ implies a long period modulation of the ordered moments the number of distinct fields may rise appreciably.

Experimentally a small commensurate $\mathbf{k}$ may not be distinguishable from a situation where $\mathbf{k}$ is incommensurate with the lattice periodicity. Both cases give rise to characteristic satellites in the magnetic neutron diffraction pattern. An incommensurate propagation vector $\mathbf{k}$ implies in principal that there will be no two sites $\mathbf{r}_i, \mathbf{r}_j$ where the ordered moments will have the same absolute value and direction. Hence, also there will be no two μ^+-sites which are magnetically identical. The effect will be a wide and smooth distribution of fields over otherwise crystallographically equivalent μ^+-positions with drastic consequences for the μSR-signal. The simplest possibility is a single-$\mathbf{k}$ sinusoidally modulated field-distribution $\mathbf{B}(\mathbf{r}) = \mathbf{B}_0 \sin(\mathbf{k} \cdot \mathbf{r})$. Muons exposed to this modulation with $\mathbf{P}_\mu(0)$ perpendicular to $\mathbf{B}_0$ will produce a μSR-signal

$$P(t) \;=\; \int \cos\left(\omega(\mathbf{r})t\right) dr = \int \cos\left(\gamma_\mu B_0 t \sin(\mathbf{k} \cdot \mathbf{r})\right) dr = J_0(t), \tag{3.4}$$

where $J_0(t)$ is the zeroth order Bessel function. The spectral distribution of $B(\mathbf{r})$ is

$$f(B) = \frac{B_0}{k} \frac{1}{\sqrt{1 - (B/B_0)^2}}. \tag{3.5}$$

The spectral distributions of some multiple-$\mathbf{k}$ incommensurate arrangements are displayed in Figure 3.1 (Apih *et al.*, 1998). They have to be calculated numerically.

Since

$$J_0(t) \propto \cos\left(\omega t - \frac{\pi}{4}\right) \qquad \text{for} \quad t \gg 0, \tag{3.6}$$

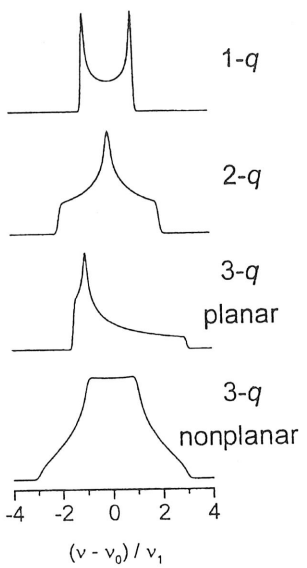

Figure 3.1. *Calculated spectral distributions for in-commensurately modulated plane waves with single or multiple propagation vectors (adapted from Apih et al., 1998).*

we detect the presence of the $J_0(t)$ term by finding in the $\cos\omega t$-fit a phase shift of the order of $\pi/4$. So far the nicest observation of a $J_0(t)$ in a μSR-signal was achieved in $CeAl_3$, (Figure 3.2). In the calculation of $B(\mathbf{r})$ or $f(B)$ it is the dipolar fields at the

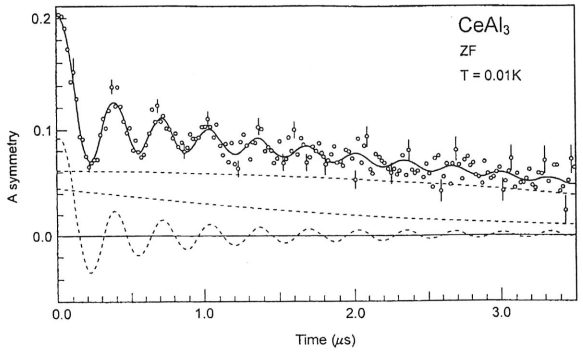

Figure 3.2. *ZF-μSR signal observed in $CeAl_3$ at 10mK. The wiggling component is best fitted with a zeroth order Bessel-function (from Amato 1997).*

μ^+-sites stemming from the modulated moments which must be primarily considered.

Recently Markus Pinkpank and Daniel Andreica have found a simplified way to calculate the distribution of $\mathbf{B}^{\mathrm{D}}$ over sites which are magnetically equivalent save for the modulation of the moment values. The dipole field $\mathbf{B}^{\mathrm{D}}$ produced by the moments $\mathbf{m}_i$,

located at sites $\mathbf{R}_i$ at the μ^+ at site $\mathbf{r}_\mu$ is as usual given by

$$\mathbf{B}^{\mathrm{D}} = \sum_i \left(\frac{\mathbf{m}_i}{r_i^3} - \frac{3(\mathbf{m}_i \cdot \mathbf{r}_i)\mathbf{r}_i}{r_i^5} \right), \quad \mathbf{r}_i = \mathbf{R}_i - \mathbf{r}_\mu \tag{3.7}$$

where

$$\mathbf{m}_i = \mathbf{m}_0 \cos\left(2\pi\mathbf{k} \cdot \mathbf{R}_i + \varphi_i\right), \tag{3.8}$$

with $\mathbf{k}$ the propagation vector. Then

$$\begin{aligned}
\mathbf{B}^{\mathrm{D}} &= \sum_i \cos(2\pi\mathbf{k} \cdot \mathbf{R}_i + \varphi_i) \left(\frac{\mathbf{m}_0}{r_i^3} - \frac{3(\mathbf{m}_0 \cdot \mathbf{r}_i)\mathbf{r}_i}{r_i^5} \right), \\
&= \cos(2\pi\mathbf{k} \cdot \mathbf{r}_\mu) \sum_i \cos(2\pi\mathbf{k} \cdot \mathbf{r}_i + \varphi_i) \left(\frac{\mathbf{m}_0}{r_i^3} - \frac{3(\mathbf{m}_0 \cdot \mathbf{r}_i)\mathbf{r}_i}{r_i^5} \right) \\
&\quad - \sin(2\pi\mathbf{k} \cdot \mathbf{r}_\mu) \sum_i \sin(2\pi\mathbf{k} \cdot \mathbf{r}_i + \varphi_i) \left(\frac{\mathbf{m}_0}{r_i^3} - \frac{3(\mathbf{m}_0 \cdot \mathbf{r}_i)\mathbf{r}_i}{r_i^5} \right), \qquad (3.9) \\
&= \mathbf{C} \cos(2\pi\mathbf{k} \cdot \mathbf{r}_\mu) + \mathbf{S} \sin(2\pi\mathbf{k} \cdot \mathbf{r}_\mu). \qquad (3.10)
\end{aligned}$$

Since we consider only magnetically equivalent sites the sums $\mathbf{C}$ and $\mathbf{S}$ are the same for all these sites. The modulation of $\mathbf{B}^{\mathrm{D}}$ over these sites depends only on $\mathbf{r}_\mu$. Equation 3.10 describes actually an ellipse and $\mathbf{B}^{\mathrm{D}}$ is the radius vector from the origin to a point on the ellipse. For an incommensurate $\mathbf{k}$ and a sufficiently larger number of equivalent sites every possible point on the ellipse may be reached. For a commensurate $\mathbf{k}$ only a few distinct $\mathbf{B}^{\mathrm{D}}$ will occur. This calculation has to be repeated for each magnetically inequivalent site. Equation 3.70 is also useful to calculate the precession cone for each $\mathbf{r}_\mu$. The Bessel function $J_0(t)$ seems to describe ZF-μSR signals in UNi_2Al_3, $CeAl_2$, $(TMTSF)_2PF_6$, and possibly others.

3.2 μSR-spectroscopy as a complement to neutron scattering

I think it is intuitively clear that, once a magnetic structure is known, one can predict the local field at the μ^+ position, but in turn it is not possible to unambiguously derive the magnetic structure from measured local fields. This is so because the μ^+ only senses the magnetic fields created by nearest neighbours and the long range properties of the magnetic structure are beyond the reach of a local probe technique. In this respect elastic neutron scattering is by far a superior technique, since it works in reciprocal space and the diffraction pattern is the better developed the longer the range of the magnetic order or, in other words, the longer the correlation lengths is. If, on the other hand, the correlation length is very short the diffraction peaks will broaden and eventually disappear while the μ^+ continues to sense more or less unchanged local fields. But even if the magnetic structure is truly long range, it may be rather complex in which case the diffraction pattern (intensities and peak positions) may no longer be uniquely correlated with a particular structure, *e.g.* multiple-$\mathbf{k}$ structure. It is then worthwhile to apply μSR-spectroscopy. Locally, different models, explaining the neutron data, may lead to quite different fields. In addition, when using single crystals μSR will also allow to determine the directions of the internal fields with respect to the crystal frame (may not work in cubic and multi domain crystals).

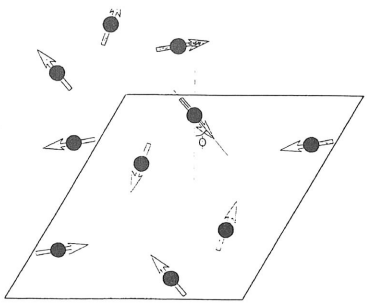

Figure 3.3. *Moment arrangement in the AF-ordered phase of $U_{14}Au_{51}$ according to Brown et al., 1997.*

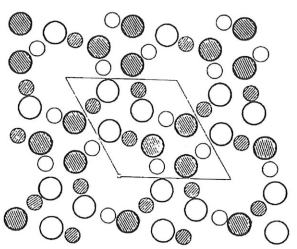

Figure 3.4. *Moment arrangement in the $U_{14}Au_{51}$ according to Dommann et al., 1990. See text for legends.*

A good example in question is provided by the system $U_{14}Au_{51}$ which was already discussed in Section 2.7. As mentioned there, the μ^+ is found at two crystallographically different sites both located in the $z = 1/2$ plane (see Figure2.12).

The results of the latest magnetic structure determination by neutron scattering is shown in Figure 3.3 (Brown *et al.*, 1997). The moments are arranged in the (a, b) plane in a kind of hexagonal star both in the $z = 0$ plane (U2-atoms) and the $z = \frac{1}{2}$ plane (U1-atoms). The ordered moments of the U1-atoms and the U2-atoms are different (μ(U1) $= 2.1\mu_B$, $\mu(U_2) = 1.35\mu_B$), the U3-atoms carry no ordered moment. An earlier neutron scattering experiment came to a different conclusion (Dommann *et al.*, 1990): again no moment at the U3-sites, and different moments at the U1- and U2-sites, ($\mu(U_1) = 0.5\mu_B, \mu(U_2) = 1.6\mu_B$), but the moment directions are parallel to the c-axes and the overall AF-structure is more simple as depicted in Figure 3.4. In the figure large and small circles designate the U2 and U1 atoms. Open and hatched circles refer to moments parallel and antiparallel to the c-axis.

ZF-μSR measurements (Schenck *et al.*, 1998) below $T_N = 22$K yielded a signal which turned out to be composed of two oscillating components with different frequencies (see Figure 3.5 and Figure 3.6) and a small third non-wiggling but relaxing component. The two oscillating components accounted for 90% of the total polarisation. this implies that the initial μ^+-polarisation $\mathbf{P}_\mu(0)$ was essentially oriented perpendicular to the two internal fields $\mathbf{B}_i$ and since $\mathbf{P}_\mu(0)$ was oriented nearly parallel to the c-axis it follows that the $\mathbf{B}_i$ are confined to the (a, b)-plane.

Adapting either of the two suggested structures we calculated the expected field maps in the $z = 1/2$ plane and searched for those positions at which the calculated B_i agreed with the measured ones. Figure 3.7 and Figure 3.8 display corresponding contour plots using either the structure of Dommann *et al.* or the structure of Brown *et al.* Indicated on these plots are also the μ^+-sites as determined from the μ^+-Knight shift according to Section 2.3. We see that the measured fields can only be reproduced with the non-collinear structure of Brown *et al.*, (1997). Also the measured direction of the internal fields $\mathbf{B}_i$ is only compatible with the ordered moments lying in the (a, b)-plane. If the structure of

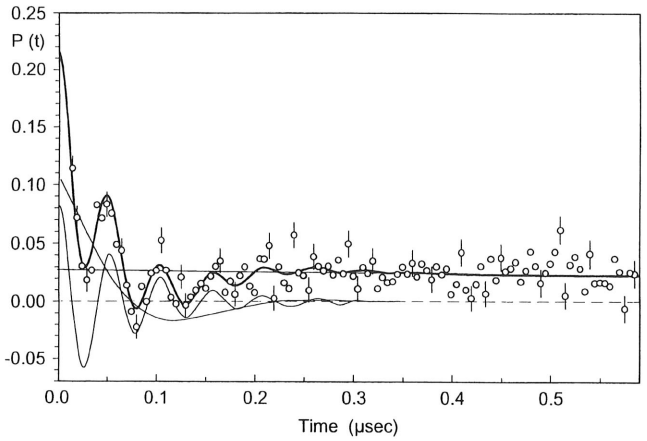

Figure 3.5. *ZF-μSR signal in $U_{14}Au_{51}$ at 19K. ($T_N = 22$ K) (Schenck et al., 1998).*

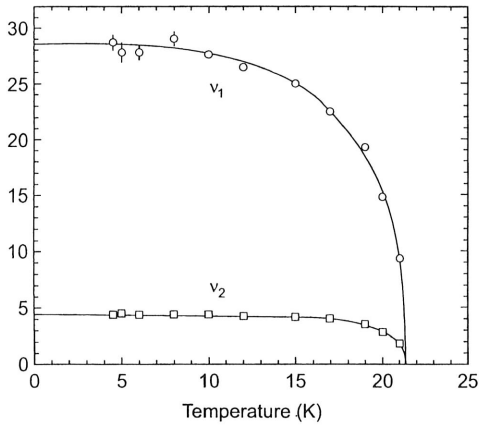

Figure 3.6. *Temperature dependence of the two spontaneous frequencies below T_N in $U_{14}Au_{51}$. The solid lines represent fits of Eq. 3.11 to the data (Schenck et al., 1998).*

Dommann *et al.* were present the $\mathbf{B}_i$ should be parallel to the c-axis. The example shows that even a qualitative feature of the μSR-signal could be sufficient to rule out a certain proposed magnetic structure.

In passing we note that the temperature dependence of the spontaneous frequencies is well fitted by the expression

$$\omega = \omega_0 \left(1 + (T/T_N)^{\delta}\right)^{\beta} \tag{3.11}$$

with $\delta \cong 3.2$ and $\beta = 0.34(3)$. The parameter β is a critical parameter which describes the order parameter near the phase transition and depends on the type of the spin-spin coupling and its dimensionality (*e.g.* 3D-Heisenberg ($\beta = 0.38$), 3D-Ising ($\beta = 0.312$), 2D-Ising ($\beta = 0.125$)). Unfortunately the measured β is not accurate enough to decide

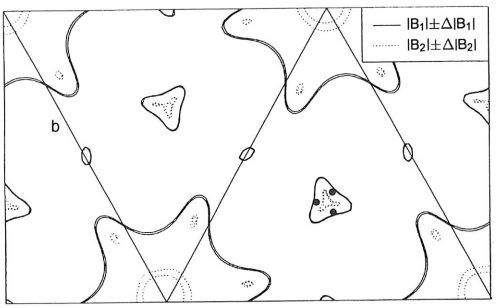

Figure 3.7. *Calculated contour lines on the basis of the structure of Brown et al., (1997) corresponding to the measured B_i in the $z = \frac{1}{2}$ plane. Note the coincidence with the known μ^+-sites. (Schenck et al., 1998).*

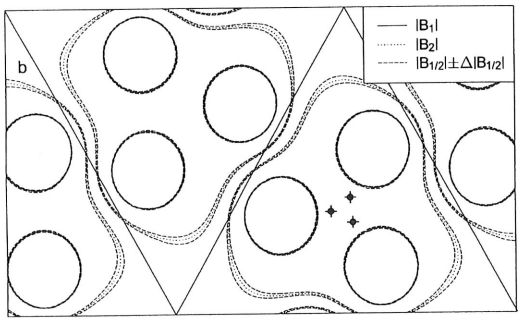

Figure 3.8. *Calculated contour lines on the basis of the structure of Dommann et al. (1990) corresponding to the measured B_i. There is no overlap with the known μ^+-sites. (Schenck et al., 1998)*

whether the 3D-Heisenberg coupling or the 3D-Ising coupling governs the magnetic behavior. The other non critical parameter $\delta(\geq 1)$ reflects magnon excitations which tend to suppress the order parameter already at low temperatures.

Now that we know that μSR can be used to confirm even quite complicated structures lets have a look on two examples where neutron scattering and μSR seem to yield incompatible structural information. (But, nota bene, these are not the only ones!)

The first example concerns CeB_6 which enters into an antiferromagnetic state below $T_N = 2.3$K. According to neutron scattering results (Effantin *et al.*, 1985) the magnetic structure is of a double-k commensurate type with a maximum moment of $0.28\mu_B$ (see Figure 3.9). We also know the μ^+-site. There is only one type of site involved, located between two Ce-atoms (*e.g.* at the position (0 0 1/2)). Calculation of the local fields on the basis of the structure seen in Figure3.9 predict seven different local fields, grouped into two narrowly split triplets and one singlet. The calculated spontaneous frequencies range from $\sim$ 4.1MHz to 12.2MHz. ZF-μSR measurements, however, reveal a completely different picture, as can be seen in Figure 3.10, displaying the Fourier transform of the μSR-signal. There are eight well resolved components extending from 2.7MHz up to

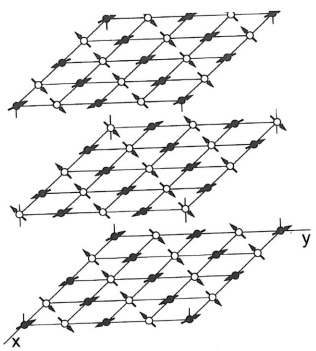

Figure 3.9. *Magnetic structure of CeB_6 according to Effantin et al., 1985.*

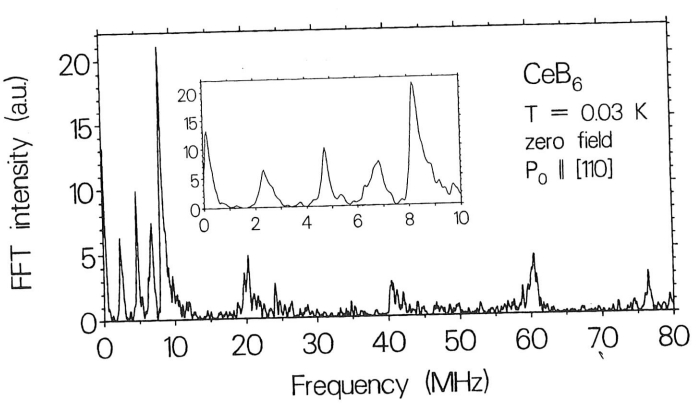

Figure 3.10. *Fourier power spectra of the ZF-μSR signal in CeB_6 below T_N. (Feyerherm et al., 1994).*

76MHz at 60mK. There is not only a problem with the suggested structure but also with the magnitude of the ordered moment. Whatever moment arrangement is assumed for the μ^+ nearest Ce-neighbours it is impossible to find a frequency as high as 76MHz.

The other example concerns the high temperature superconductor $HoBa_2Cu_3O_7$. In this compound the Ho-4f moments enter into a 3D-long range AF-order below 190mK (Roessli *et al.*, 1993). Above that temperature a 2D-order, confined to the Ho-plane is observed. According to neutron diffraction work (Roessli *et al.*, 1993) the low temperature value of the ordered moment amounts to $2.8\mu_B$ and the AF-structure is described by a single propagation vector $\mathbf{k} = (0\ \frac{1}{2}\ \frac{1}{2})$, *i.e.* the magnetic unit cell is doubled along the b- and c-direction and the moments are arranged ferromagnetically along the a-direction. The μ^+-position in $YBa_2Cu_3O_7$ is known to be near a chain oxygen at a distance of ~ 1Å(Weber *et al.*, 1990). Using the structure of Roessli *et al.*, and performing dipolar field calculations for the mentioned site (there is no contact contribution in this oxide) one predicts a field of 6.4G while the measured field is of the order of 200G. (Birrer *et al.*, 1989; M. Pinkpank, private communication, see Figure 3.11). Obviously we have a problem here. But who or what is to blame? We don't know yet.

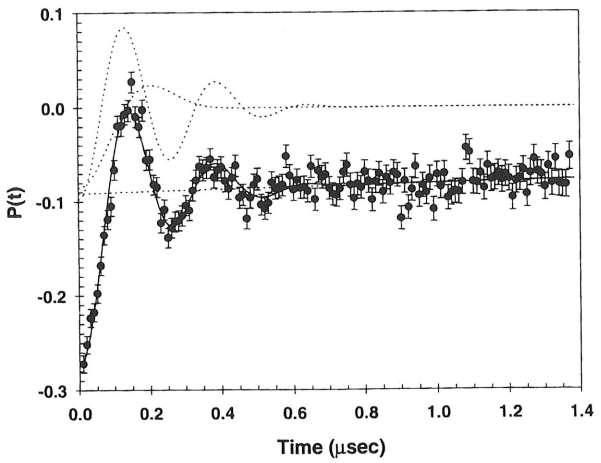

Figure 3.11. *ZF-μSR signal in $HoBa_2Cu_3O_7$ at 50mK. The rapidly wiggling component corresponds to a field of* ~ 240 *G. (M. Pinkpank, private communication).*

3.3 Ultra small moment magnetism in heavy fermion systems

This lecture should not end without touching on another very important facet of the μSR technique, namely its potential for detecting rather weak magnetic fields down to the order of 0.5G and correspondingly small magnetic moments. We know that the dipolar field distribution from nuclear moments can readily be monitored. Hence it should be possible to detect also very small moments of electronic origin. Very small moments of electronic origin may be expected in Kondo lattice systems where the Kondo effect nearly but not completely screens the local moments or in systems showing itinerant or band magnetism. Experimentally it is not really possible to distinguish a small distinct field from a distribution of very small fields since for $\omega t \ll 1$

$$\cos \omega t \simeq 1 - \frac{1}{2}(\omega t)^2 \simeq \exp\left(-\frac{1}{2}(\omega t)^2\right). \tag{3.12}$$

Also the Gaussian function for very small arguments is hardly distinguishable from an experimental decay when fitting some data. Another problem is to decide whether a slowly relaxing signal in ZF reflects static or dynamic features. Usually a distinction can be made by performing LF measurements. But Dalmas de Reotièr *et al.* (1998) have recently discussed cases where the dynamics may be suppressed by small magnetic fields if the magnetic excitations are in the 10neV range. Since the system doesn't care whether a LF or TF-geometry is used suppression of the dynamically induced relaxation should be visible in a TF-experiment, while a static distribution should not be much affected.

The best example for the appearance of some ultra small moment magnetic order is probably seen in the heavy electron compound $CeRu_2Si_2$. Figure 3.12a displays the temperature dependence of the ZF-relaxation rate λ (using an exponential decay function). The rates are tiny but a clear increase of λ is seen below 2K. In longitudinal fields this increase is quenched. If the increase of λ is interpreted as reflecting the development of a static field distribution ($\Delta B \sim 0.2$G) and taking into consideration the known μ^+-position

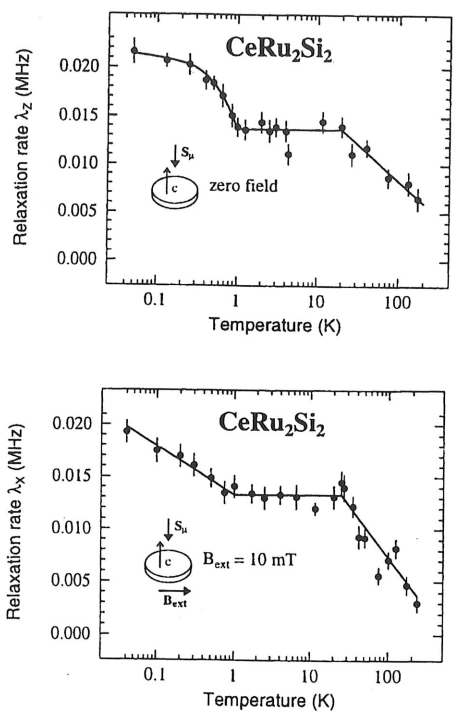

Figure 3.12. *(a) Temperature dependence of ZF-relaxation rate λ in $CeRu_2Si_2$, (b) temperature dependence of TF-relaxation rate (Dalmas de Reotièr et al., 1998).*

in this compound one estimates for the size of the moments a value of $\sim 10^{-3}\mu_B$ (Note that the proton nuclear moment has a value of $\sim 3 \times 10^{-3}\mu_B$) Nothing, of course, can be said, about the magnetic structure, but it may not be unreasonable to imagine it as an incommensurate modulated structure (Amato et al., 1994). This may also allow to understand why the relaxation function seems to be an exponential. The definite proof, that dynamics is not involved is provided by recent TF-measurements ($H_{\text{ext}} = 100$Oe) by Dalmas de Reotèr *et al.* (1998), see Figure 3.12b. Again below 2K λ_{TF} increases. These data are more accurate since they were obtained at the pulsed muon source of ISIS.

Another interesting example is seen in the famous heavy fermion superconductor $U_{1-x}Th_xBe_B$. The superconducting phase diagram is shown in Figure 3.13. In the doping range $1.9\% < x < 4.2\%$ two phase transitions show up as revealed by specific heat measurements. The upper transition temperature T_{c1} is still associated with the onset of the superconducting state, while the nature of the lower T_{c2} was unknown. ZF-μSR measurements (Heffner *et al.*, 1989) revealed a pronounced increase of the ZF-relaxation rate σ (this time best described by a Gaussian relaxation function) as the temperature was lowered below T_{c2} as can be seen in Figure 3.14.

Note that σ is already quite high above T_{c2}, in contrast to the situation in $CeRu_2Si_2$. This is due to the Be nuclear dipole fields which produce a field distribution at the μ^+-sites with a width of the order of 2.8G. The broadening below T_{c2} amounts to about 2G. Apparently the phase below T_{c2} besides being superconducting is associated with

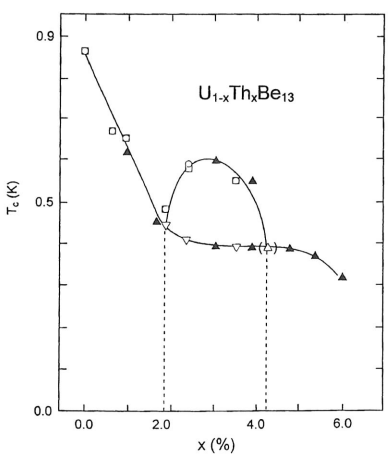

Figure 3.13. *Superconducting phase diagram of $U_{1-x}Th_xBe_{13}$.*

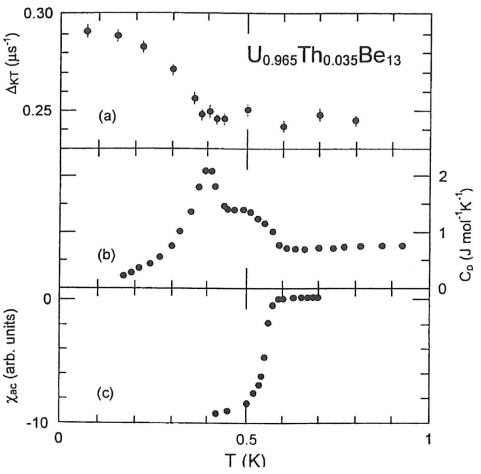

Figure 3.14. *Temperature dependence of the μ^+-ZF relaxation rate σ, specific heat and ac-susceptibility. (Heffner 1989).*

the development of small static moments of the order of $5 \times 10^{-3}\mu_B$, probably randomly frozen. The true nature of this state is still not settled, but an interesting conjecture is that the superconducting state below T_{c2} violates time reversal invariance leading to the spontaneous appearance of spin or orbital moments (Sigrist and Rice, 1989).

Finally one cannot discuss ultra small moment magnetism without referring to another heavy fermion superconductor: UPt_3. First evidence for a magnetic state below (5-6)K came from an early μSR-experiment (Cooke *et al.*, 1986), see Figure 3.15. Since then both neutron (Aeppli *et al.*, 1989) and synchrotron radiation (Isaacs *et al.*, 1995) work has confirmed the development of antiferromagnetic order below 6K and the ordered moment was determined to be $\sim 0.02\mu_B$. Strangely enough, all further μSR-studies, on high quality single crystal samples (Figure 3.15) could not find any evidence for the presence of magnetic order. Also, using NMR, the small moment magnetic structure was not seen (Kohori *et al.*, 1990). How can this be understood?

It is well known that by substituting Th for U, or Pd for Pt normal moment AF-order is observed (*e.g.* in $U(Pt_{0.95}\ Pd_{0.05})_3$ $m = 0.62\mu_B/U$). The structure is found to be the same as in pure UPt_3. And in these doped systems also ZF-μSR measurements (de Visser *et al.*, 1997) reveal the presence of magnetic order by a typical oscillatory behavior (see Figure 3.16). The data in Figure 3.16 are excellently fitted by the 3 component function (polycrystalline sample).

$$P(t) = A_1\left(\frac{2}{3}e^{-\lambda_0 t}\cos\omega t + \frac{1}{3}e^{-\lambda t}\right) + A_2 G_{\mathrm{LKT}}(\lambda_2 t) \tag{3.13}$$

with G_{LKT} is the Lorentzian Kubo-Toyabe function, demonstrating the presence of two different μ^+-sites (or magnetic domains?) The first site is associated with a local field of ~ 590G at $T \ll T_N \simeq 6.2$K, the second site or sites seems to show a Lorentzian field distribution with zero average. Believing in the quoted magnetic structure a zero average

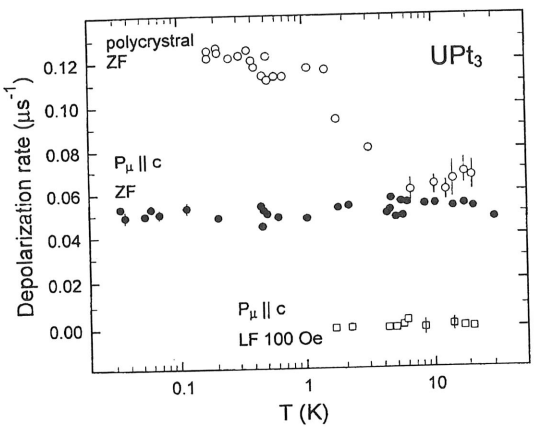

Figure 3.15. *ZF-relaxation rate in UPt_3 showing strong sample dependencies (taken from Amato, 1997) (original data are from Cooke et al. 1986 and Dalmas de Reotier et al., 1995).*

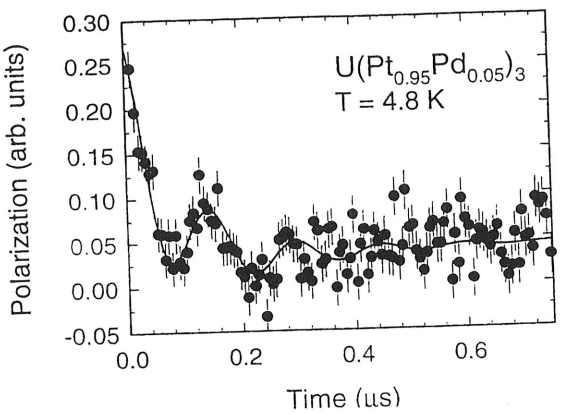

Figure 3.16. *ZF-μSR signal in $U(Pt_{0.95}Pd_{0.05})_3$. The solid line is a fit of Equation 3.13 to the data. (de Visser et al., 1977).*

field is calculated for the so called a-site (0 0 0) and a finite field at the g-site ($\frac{1}{2}$ 0 0). Rescaling the field of 590G by the moment ratio 0.02/0.62 we should have seen a field of 19G also in UPt_3, provided that the same site is occupied as in $U(Pt_{0.95}\ Pd_{0.05})_3$. Do we have any evidence for a two site occupation in UPt_3 from Knight shift measurements? There may be some small splitting in the TF-signal, but there are conflicting results from measurements on different samples. In any case if the g-site should be occupied one expects a sizable spitting into up to 3 components which is definitely not seen, also not in measurements of the Knight shift in a single crystal of $U(Pt_{0.95}\ Pd_{0.05})$. The appearance of two signals in the ordered state of $U(Pt_{0.95}\ Pd_{0.05})_3$ remains a mystery and hence cannot be used to help solving the puzzling absence of any signature for the small moment ordered state in the μSR-signal. But may be, the explanation has to be searched for elsewhere.

The fact that also NMR does not reveal the ordered state, although at the Pt-site one expects a field of 900G, has led to the suggestion that the moments in UPt_3 fluctuate with a correlation time, long compared to the neutron time window, but short on the time scale of NMR and μSR-spectroscopy. This example illustrates I believe in an exemplary fashion the types of problems one may encounter in a μSR-study when trying to reconcile different aspects of the experimental results not only from μSR measurements but also from other techniques such as NMR and neutron-scattering. In the end if consistency can be achieved one has truly expanded a bit our understanding of how nature works in some particular case. Maybe it is only a small step forward, but progress is often only achieved step by step, like learning how and when to apply μSR-spectroscopy.

References

Abragam A, 1970, *The Principles of Nuclear Magnetism* (Oxford Univ Press, London).
Abrikosov A A, 1972, *Introduction to the Theory of normal Metals* (Academic Press, NY).
Akishin P G, Gaganov I A, 1992, *J Magn Magn Materials* **110** 175.
Amato A *et al.*, 1992, *Solid State Communic* **82** 767.
Amato A *et al.*, 1994, *Phys Rev* **B50** 619.
Amato A *et al.*, 1997, *Revs Mod Phys* **69** 1119.
Apih T *et al.*, 1998, *Phys Rev Lett* **80** 2225.
Baumann D *et al.*, 1986, *Hyperfine Interact* **31** 455.
Birrer P *et al.*, 1989, *Phys Rev* **B39** 11449.
Boon M H, 1964 *Physica* **30** 1326.
Brown P J *et al.*, 1997, *J Phys.: Condens Matter* **9** 4729.
Carter G C, Bennet L H and Kahan D J, 1977, *Metallic Shifts in NMR*, Progr in Mater Science, **Vol. 20** (Pergamon, Oxford).
Condon J H, 1966, *Phys Rev* **145** 526.
Condon J H, Walstedt R E, 1968, *Phys Rev Lett* **21** 612.
Dalmas de Reotièr P *et al.*, 1995, *Phys Lett* **A205** 239.
Dalmas de Reotièr P, Yaouanc A, 1997, J Phys.: Condens Matter **9** 9113
Dalmas de Reotièr P *et al.*, 1998, *Contribution to SCES'98* (Paris).
Davies D W, 1967, *The Theory of Electric and Magnetic Properties of Molecules* (Wiley, New York).
Dommann A *et al.*, 1990, *J Less Common Met* **160**, 171.
Doniach S, 1977, *Physica* **91 B** 231.
Effantin J M *et al.*, 1985, *J Magn Magn Mater* **47 & 48** 145.
Feyerherm R *et al.*, 1994a, *Phys Rev Lett* **73** 1849.
Feyerherm R *et al.*, 1994b, *Physica B* **194-196** 357.
Feyerherm R, 1995, Thesis No 11249 ETH Zürich.
Feyerherm R *et al.*, 1995, *Z Physik* **B99** 3.
Gygax F N *et al.*, 1984, *J Less Common Met* **101** 97
Gygax F N *et al.*, 1986, *Phys Rev Lett* **56** 2842
Hayakawa H et al, 1988, *J Less Common Met* **143** 315.
Heffner R H *et al.*, 1989, *Phys Rev* **B40** 806.
Jones W and March N H, 1973, *Theoretical Solid State Physics* Vol. I (Dover, New York).
Kittel C 1966 *Quantum Theory of Solids* (Wiley, New York).
Knetsch E A *et al.*, 1993 ,*Physica* **B186-188** 300
Kyogaku M *et al.*, 1993, *J Phys Soc Jpn* **62** 4016.
Lovesey S W, Cuccoli A, Tognetti V, 1990, *Hyperfine Interactions* **64** 321

Manninen M, Nieminen R, 1979, *J Phys F: Met Phys* **9** 1333.
Manninen M, 1983, *Phys Rev* **B27** 53.
Moriya T, 1963,*J Phys Soc Jpn* **18** 516.
Roessli B *et al.*, 1993, *Europhys Lett* **23** 511.
Rubens A *et al.*, 1973, *Phys Rev* **B7** 105.
Schenck A, 1981, *Helv Physica Acta* **54** 1982.
Schenck A, 1993, in *Frontiers in Solid State Sciences*, Vol 2, edited by L.C Gupta, M.S Murani (Wold Scientific, Singapore) p 269.
Schenck A, Gygax F N, 1995, in *Handbook of Magnetic Materials*, Vol 9, edited by Buschow K H J (Elsevier, Amsterdam) p 57.
Schenck A *et al.*, 1998, *J Phys.: Condens Matter* **10**, 1.
Sigrist M, Rice T M, 1989, *Revs Mod Phys* **63** 239.
Solt G *et al.*, 1996, *Phys Rev Lett* **76** 2575 and to be published (1998).
de Visser A *et al.*, 1997, *Physica* **B230-232** 53.
Wachter P *et al.*, 1995, *Phys Rev* **B51** 5542.
Weber M *et al.*, 1990, *Hyperfine Interact* **63** 207.
Weinert R W, Schumacher R T, 1968, *Phys Rev* **172** 711
Wiesinger G *et al.*, 1995 *Physica* **B206-207** 261
Wiesinger G *et al.*, 1997, *Physica* **B230-232** 243
Yosida K, 1958, *Phys Rev* **110** 769
Zaremba E, Zobin D, 1980, *Phys Rev* **B22** 5490.